The closer, the better: intratumoral delivery of a thermoresponsive gemcitabine-loaded hydrogel in preclinical PDAC models

Vallés-Martí, A.; Manelkar, A.; Simpson, C.R.; Kinderman, P.; Jonge-Muller, E. de; Wielen, A. van der; ... ; Hawinkels, L.J.A.C.

Drug Delivery and Translational Research
https://doi.org/10.1007/s13346-026-02187-6

ORIGINAL ARTICLE

The closer, the better: intratumoral delivery of a thermoresponsive gemcitabine-loaded hydrogel in preclinical PDAC models

Andrea Vallés-Martí[1] · Ajinkya Manelkar[1] · Christopher R. Simpson[2,3] · Priscilla Kinderman[1] · Eveline de Jonge-Muller[1] · Anthea van der Wielen[1] · Stefanus G.T. Janson[1] · Ahmad Alrawahneh[2] · Li Zihao[2,3] · Tushar Tomar[3] · Mike G.W. de Leeuw[3] · Helena M. Kelly[2,3,4] · Lukas J.A.C. Hawinkels[1]

Received: 12 September 2025 / Accepted: 10 July 2026

Abstract

Current treatments for pancreatic ductal adenocarcinoma (PDAC) patients are typically restricted to (neo)adjuvant chemotherapy, surgery or palliative care. Mainly due to a late diagnosis and highly desmoplastic environment, these treatments have limited efficacy and patient prognosis is very poor. Intratumoral delivery of chemotherapeutic agents using hydrogel technology might boost treatment efficacy and reduce side effects. Here, we aimed to investigate the preclinical efficacy and tolerability of a novel thermosensitive hydrogel, *ChemoGell*, loaded with the chemotherapeutic agent gemcitabine. We explored this in vitro, using patient-derived organoids and surgically obtained tumor explants, and in vivo, using a human patient-derived xenograft (PDX) and syngeneic KPC3 mouse models. Upon intratumoral injections of gemcitabine-loaded ChemoGell, respective survival, peripheral blood and end-stage tumor histological analyses were performed. Intratumoral injection of gemcitabine-loaded ChemoGell in in vitro and in vivo models showed decreased tumor growth and increased cytotoxicity compared to blank ChemoGell and saline control intratumoral injections. In contrast, systemic administration of gemcitabine did not show therapeutic benefits. Intratumoral ChemoGell injections induced interesting lymphocyte and monocyte dynamics overtime, showing an intratumoral influx of NK cells and monocytes and an in-depot infiltration of activated fibroblasts, macrophages and activated CD8+T cells. Our findings establish a foundation for integrating localized treatment modalities, addressing critical challenges in PDAC and improving patient prognosis through more effective, localized therapeutic strategies.

Keywords Pancreatic cancer · Intratumoral treatment · Gemcitabine · Drug delivery · Thermoresponsive drug-loaded hydrogel

Background and aims

Cancer mortality has been declining for most cancers in the past years, except for pancreatic ductal adenocarcinoma (PDAC), which keeps rising in global mortality rankings, and is predicted to become the second leading cause of cancer by 2030 [1]. This is largely due to late diagnosis, high invasiveness, cellular heterogeneity, poor vascularization, and a lack of effective treatments. Currently, surgery remains the only potentially curative treatment [2]. However, as the majority of patients present with distant metastasis at the time of diagnosis, only a limited number are eligible for surgical resection (10–25%). For those with resectable tumors, chemotherapy is typically administered both pre- and post-operatively. In cases of locally advanced or metastatic PDAC, only systemic chemotherapy is given,

Andrea Vallés-Martí, Ajinkya Manelkar and Christopher R. Simpson contributed equally to this work.

✉ Lukas J.A.C. Hawinkels
l.j.a.c.hawinkels@lumc.nl

[1] Department of Gastroenterology and Hepatology, Leiden University Medical Center, Leiden, Zuid-Holland, The Netherlands

[2] School of Pharmacy and Biomolecular Sciences, Royal College of Surgeons in Ireland (RCSI), Dublin, Ireland

[3] OncoLize B.V., Maastricht, The Netherlands

[4] Tissue Engineering Research Group, Department of Anatomy, Royal College of Surgeons in Ireland (RCSI), Dublin, Ireland

Published online: 18 July 2026

typically consisting of either gemcitabine plus nab-paclitaxel or FOLFIRINOX (a combination of fluorouracil, leucovorin, irinotecan, and oxaliplatin) [3]. These treatments have limited efficacy, with only a few months survival benefit [4, 5] and a high number of serious adverse events. These side effects can significantly affect patient's quality of life and influence disease progression, especially when other comorbidities are present [6].

Part of the poor efficacy of systemically applied drugs might be due to poor penetration of drug into the tumor after systemic delivery, caused by poor vasculature and the desmoplastic tumor microenvironment in PDAC [7–10]. Localized therapeutic delivery systems have been shown to improve this by enhancing local drug concentrations, while reducing the systemic side effects. However, a challenge with this approach is the fast drug clearance from the tumor site [11, 12]. In addition, despite numerous iterations of intratumoral formulation strategies, there are key barriers hindering clinical translation such as uncertainty surrounding the use of novel excipients or therapeutic cargos, manufacturing at scale, drug loading, delivery systems and dosing regimens, and overall efficacy of the strategy [13].

To address these challenges, poloxamer-based thermoresponsive hydrogels have been tested (pre)- clinically for multiple solid tumors [14–17]. These hydrogels can encapsulate drugs and are low-viscosity polymer dispersions at room temperature that transition into semisolid depots when approaching body temperature (37 °C). By forming a drug-depot, drug retention is ensured within the tumor mass.

ChemoGell (CG) is a novel patented thermoresponsive polymer system that can be loaded with both hydrophilic and hydrophobic chemotherapeutic drugs [12, 18]. It has been shown to be easily injectable at room temperature using standard injection equipment, while undergoing a sharp state transition to a semi-solid depot upon approaching body temperatures in vivo. Uniquely, CG further chemically cross-links after its sol-gel transition, increasing the gel strength in the first 24–48 h. This reduces the rate of disintegration, increasing the duration for which the depot is retained in situ, allowing sustained drug delivery. The CG system has been previously evaluated in vivo in an A549 xenograft mouse model [12]. In this study, it was shown to significantly reduce tumor volume relative to saline, with an unloaded or empty CG platform, showing some inherent anti-tumor properties. Additionally, the formulation was well tolerated, and no adverse effects were observed.

PDAC presents a tumor that may particularly benefit from intratumoral delivery in light of its avascular and desmoplastic nature. Therefore, the CG platform has been reformulated incorporating gemcitabine (ChemGem), a gold standard chemotherapeutic in the treatment of PDAC. Direct intratumoral injection of ChemGem could have potential clinical applications in PDAC both neoadjuvantly to reduce tumor burden prior to surgery improving resection outcomes, and in later stages to control tumor growth providing symptomatic relief and improved quality of life outcomes.

In this study, we aim to evaluate the effectiveness and tolerability of blank and gemcitabine loaded ChemoGell, for treating PDAC in syngeneic KPC3 and human patient derived xenograft (PDX), organoid and explant PDAC models. In addition to cytostatic effects, we further investigate the effects on the tumor microenvironment. Our data show improved therapeutic outcomes and provide new avenues for the combination of systemic and local treatments.

Results

ChemoGell with gemcitabine (ChemGem) maintains injectability and thermoresponsivity providing robust depot formation

To understand the physical performance changes of CG when incorporating gemcitabine HCl, rheological and disintegration analysis comparing CG and ChemGem. Gemcitabine release testing was also used to discern the effects of environmental pH on CG gelated integrity and gemcitabine release. Gemcitabine HCl inclusion caused a 1 °C increase in the liquid to solid state transition temperature of ChemoGell from 25.64 °C to 26.61 °C (Fig. 1B). This increase in gelating temperature translated to lowered gelated stiffnesses at 37°C, with G' values of 9432 Pa and 11,440 Pa for ChemGem and CG respectively (Fig. 1C). Additional differences were also apparent, with a lowered viscosity of 0.56 Pa.s in ChemGem and 1.52 Pa.s in CG, observed at 1.58 s-1 (Fig. 1D). CG's shear-thinning property was further observed as feasible injection via ultrafine subcutaneous needles, percutaneous biopsy needles and endoscopic ultrasound-guided fine-needle aspiration (EUS FNA) devices. These injection procedures reported respective maximum extrusion forces of 9.3 N, 4.1 N and 19.2 N at room temperature (Fig. 1E). In every case, the extrusion forces were below the lower average human pinch strength of 80 N. The ability of ChemoGell to yield a long-term stable depot in disintegration studies was observed by 2 phase-cross-linkage, an initial thermoresponsive physical association followed by permanent covalent chitosan-genipin linkage signified by a color change (Fig. 1F). Despite gemcitabine related changes in shearing physical properties, ChemGem retained the ability to form a robust semi-solid depot with an equivalent disintegration profile to ChemoGell when submerged in a neutral supernatant 37 °C. ChemGem's disintegration was influenced by changes in environmental pH (Fig. 1G),

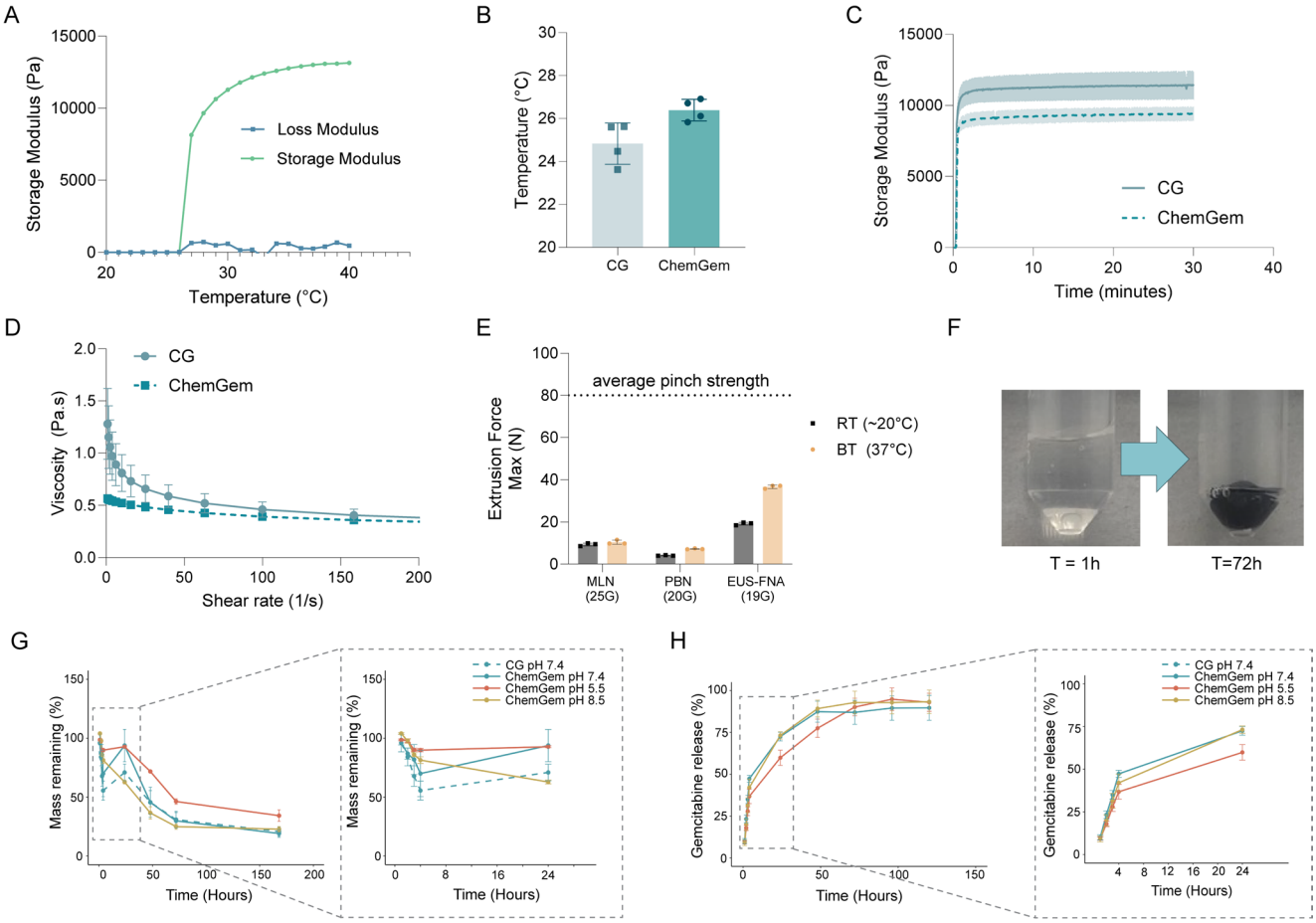

Fig. 1 Gemcitabine release and influence on rheological properties of ChemoGell. **A** Rheogram showing sol-gel transition profile of blank ChemoGell (CG). Gelation was defined as the point where the storage modulus exceeds the loss modulus. **B** Gelation temperatures of ChemoGell ($n=4$) and ChemGem ($n=4$) plotted as mean ± SD. **C** Gelated stiffness profile of ChemoGell ($n=3$) and ChemGem ($n=3$) maintained at 37 °C for 30 min. Lines represent the respective means. **D** Viscosity flow profiles as a function of increasing shear rate for ChemoGell ($n=3$) and ChemGem ($n=3$). Lines represent the respective means. **E** Maximum forces measured, at room temperature (RT) when extruding ChemoGell from syringes and a 25G MicroLance needle (MLN), a 20G Percutaneous biopsy needle, (PBN) or a 19G endoscopic ultrasound guided fine needle aspiration device (EUS-FNA). **F** Representative images of ChemoGell undergoing clear to dark blue colour change at 72 h incubation indicative of genipin-chitosan chemical linkage. **G** In vitro ChemoGell and ChemGem mass disintegration profiles when submerged at 37 °C in pH 7.4, pH 5 and pH 9 supernatants at 1-week (left) and 24-hours (right). **H** Gemcitabine release profiles from ChemGem incubated at 37 °C in pH 7.4, pH 5.5 and pH 8.5 supernatants at 1 week (left) and 24-hours (right). Graphs plotted as the mean ± SD ($n=3$)

with acidic (pH 5.5) supernatant degrading the depot more slowly compared to ChemGem in basic environments (pH 8.5). Closer analysis of the first 24 h (Fig. 1G) showed the lowest mass retention in basic environments while acidic pHs highly retained ChemoGell's depot mass. These disintegration profiles were concordant with gemcitabine release (Fig. 1H) specifically, in neutral and basic environments release was equivalent, while acidic environments yielded an overall slower gemcitabine release rate.

Intradome injections of gemcitabine-loaded ChemoGell increase cell death and impair viability in patient-derived organoids and explants

To evaluate the efficacy of gemcitabine-loaded ChemoGell (ChemGem) in vitro, intradome injections were performed on patient-derived organoids (PDOs) encapsulated in Matrigel-domes (Fig. 2A). Four PDOs, Pac09, Pac42, Pac12 and Pac60, were used. Gemcitabine is known to promote apoptosis and cell cycle arrest by inhibiting DNA synthesis [19]. Consequently, upon exposure to intradome injected ChemGem, all PDOs showed a significant increase of cell death and decrease of cell viability, measured by propidium iodide and Hoechst staining respectively (Fig. 2B, Supp.

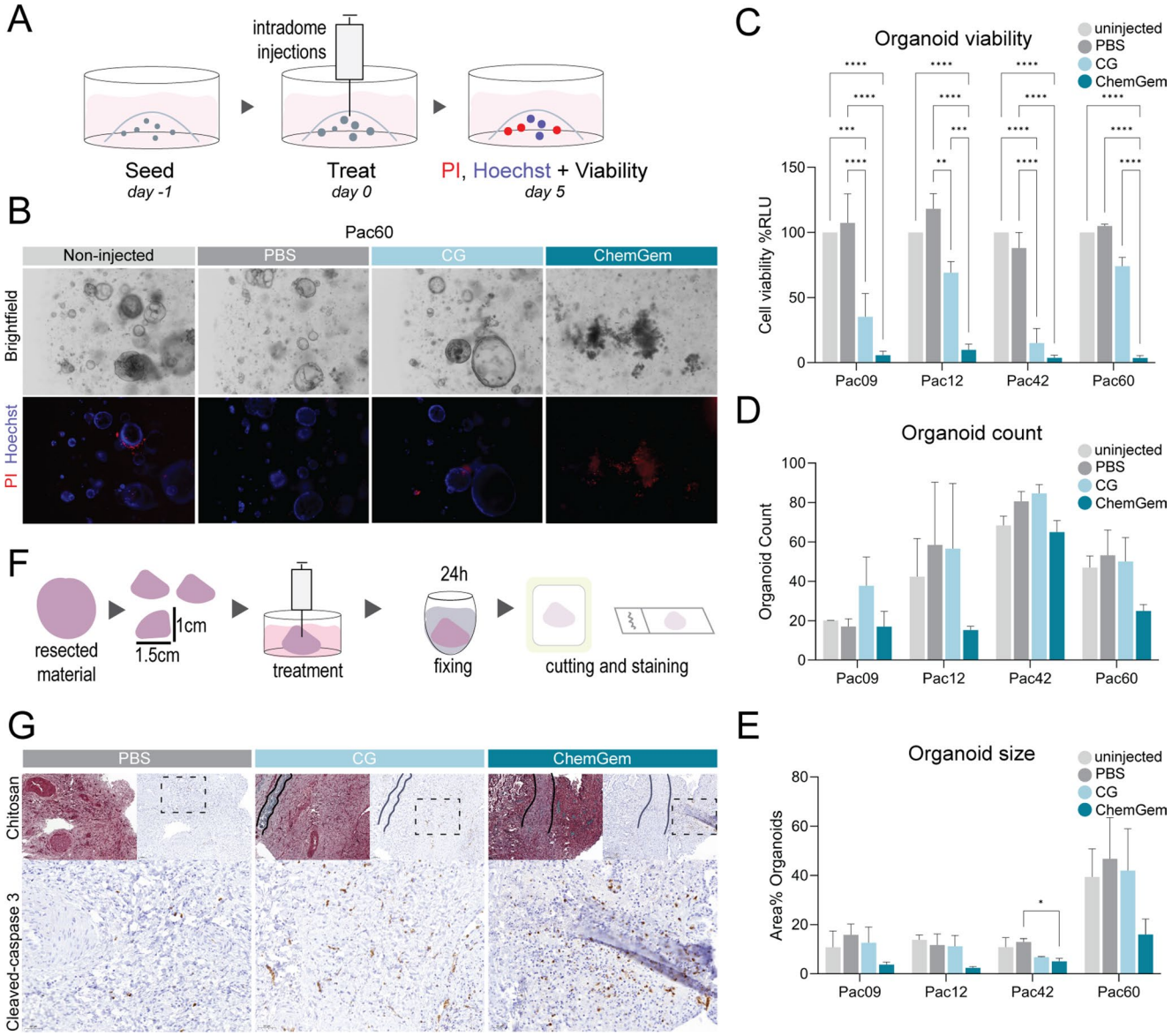

Fig. 2 Intradome and explant injections in patient-derived models. **A** Workflow of intradome injections in patient-derived organoids. After 24 h of seeding organoid fragments, intradome injections of 10 µl of PBS, CG and ChemGem were performed. Media was refreshed at day 3, and experiment was ended at day 5. **B** Brightfield and propidium iodide and Hoechst images at day 5 post treatment. **C** Organoid viability of Pac09, Pac12, Pac42 and Pac60 at day 5 measured by Cell Titer Glo. Mean±SEM, $n=3$ per patient-derived model. (**D-E**) Particle analysis at day 5 using ImageJ of **D** organoid count and **E** organoid size/area. Mean±SEM plotted, $n=3$ per patient-derived model. **F** Workflow of patient-derived explant injections and tissue fixation after 24 h of treatment. Freshly resected material was divided into 1 × 1.5 cm pieces and treated with 10 µl PBS, CG and ChemGem. After 24 h, material was fixed in PFA and processed for histological analysis. **G** Chitosan and cleaved caspase-3 stainings after 24 h of treatment in pancreatic cancer explant PaC73 with PBS, CG and ChemGem

Figure 1A) accompanied by a decrease in organoid area and count 5 days post-treatment (Fig. 2C-E). To a lesser extent, treatment with blank (non-gemcitabine containing) CG also showed a decrease in viability compared to respective PBS injected control, in line with previous observations showing chemoablative properties of empty ChemoGell [12]. Nevertheless, ChemGem was superior to empty CG in terms of viability, organoid count and size.

As organoids lack the stroma and immune compartment, which play a key role in PDAC development and treatment, surgically resected PDAC tumor tissue and normal-adjacent tissue were used to generate 1 × 1.5 cm explants and subsequently injected (Fig. 2F, Supp. Figure 1D). After 24 h, tissues were fixed and processed for histological analysis (Fig. 2G). Notably, increased cleaved-caspase 3 (CC3) staining was observed only upon CG and ChemGem, localized in the proximity of the needle track and the ChemoGell

depot as identified by chitosan staining. This was mainly observed in the PDAC tissue, and barely in the normal-adjacent tissue (Supp. Figure 1B). Overall, the in vitro and ex vivo assessment of gemcitabine-loaded ChemoGell revealed substantial cytotoxicity in PDOs and resected PDAC tissue, underscoring its potential as a targeted treatment for pancreatic cancer.

Intratumoral injections of gemcitabine-loaded ChemoGell strongly decrease human patient-derived xenograft (PDX) growth

To further evaluate the antitumor efficacy of ChemGem in vivo, we used a close-to-patient PDAC PDX model, and injected tumors when reaching a volume of 125±25mm^3 (Fig. 3). CG-depots in the tumor area were confirmed in vivo using fluorescent marker in CG 2 h after first (T1) and 2 h before second (T2) injections (Supp. Figure 2A-C). Remaining fluorescence was confirmed ex vivo at the end of the experiment (Supp. Figure 3A). Additionally, ChemoGell presence was confirmed by staining for the CG component chitosan (Supp. Figure 2D). Of note, no ChemoGell was identified ex vivo in other organs (Supp. Figure 3A).

After the first injection, tumor growth rate was significantly reduced in ChemGem treated mice, compared to exponential growth in saline, and slightly later, in CG-treated mice (Fig. 3A, B). No significant changes in weight were identified (Fig. 3C). None of the ChemGem treated mice reached the experimental endpoint and were still alive at the end of experiment. In contrast, all CG and saline treated mice tumor volumes did, with a median survival of 45 days and 25 days, respectively (Fig. 3D, ChemGem vs. CG p 0.0013). Improved survival and reduced tumor growth rates were supported by observations during necropsy, with tumor volumes being significantly reduced between in vivo and ex vivo measurements (Fig. 3E, F), mainly due to formation of fluid filled cysts within the tumors, only observed in CG and ChemGem groups (Fig. 3G).

Molecular characteristics of these end stage tumors were further investigated by HE staining, and IHC expression of pan-cytokeratin, vimentin, Ki67 and CC3 expression (Fig. 4). Although not significant, a reduction in nuclei and pan-cytokeratin was found in both CG and ChemGem treated tumors, compared to saline (Fig. 4A, B), likely associated to the slower tumor growth rates (Fig. 3A, B). An increase in vimentin expression was observed in CG and

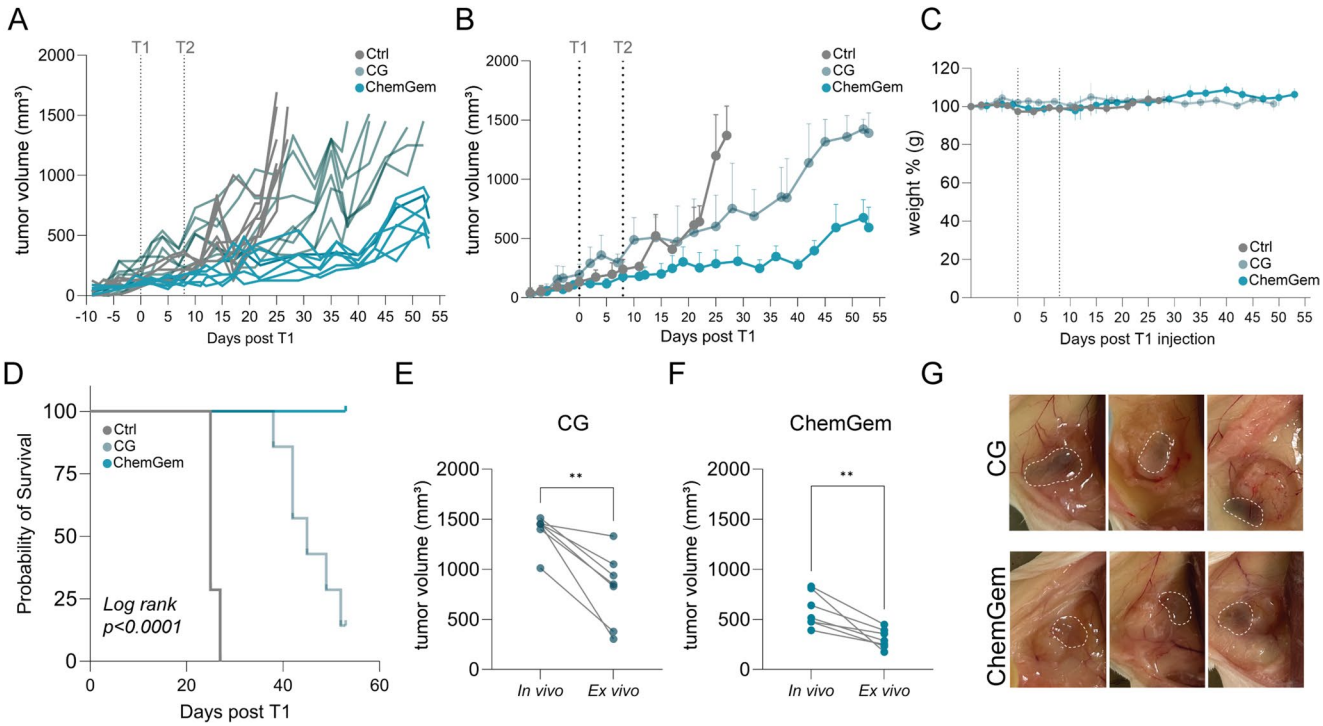

Fig. 3 Gemcitabine-loaded hydrogel reduces tumor growth and maintains survival of pancreatic cancer patient-derived xenograft. **A** Individual tumor volume overtime of mice treated with saline ($n=7$), ChemoGell (CG, $n=7$) and Gemcitabine-loaded CG (ChemGem, $n=7$), measured by a calliper. Dotted lines indicate first (T1) and second (T2) injections. **B** Tumor volume measured overtime plotted as cumulative mean±standard deviation (SD), per treatment group. **C** Mice weight progression in percentage during the experiment, normalized to starting weight. (**D**) Kaplan-Meier analysis of mice treated with ChemGem (median undefined), CG (median 45 days) and saline (median 25 days) for an 8-week period. Overall significance was determined using a log rank test ($p<0.0001$). **E**–**F** Tumor volume of (**E**) CG and (**F**) ChemGem, at humane end point in vivo (prior to dissection) and ex vivo (post dissection). **G** Representative images of cysts and hydrogel-depots in CG and ChemGem treated tumors

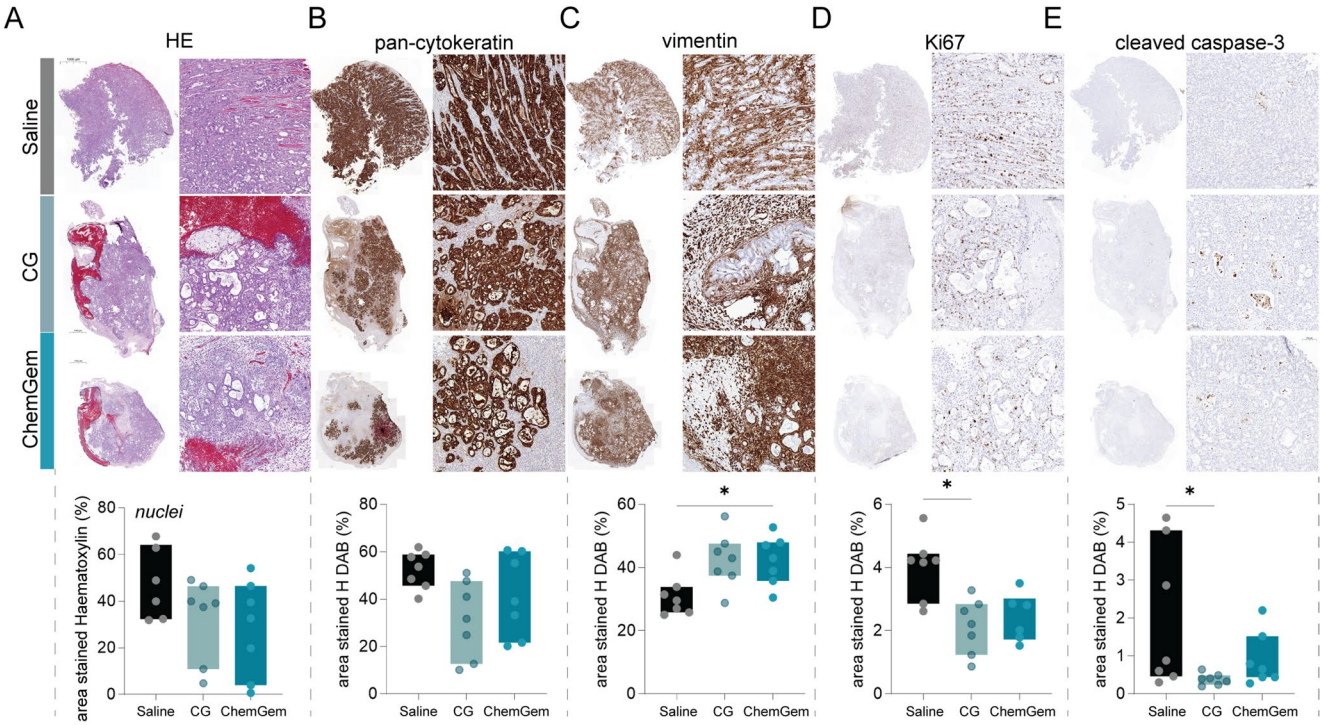

Fig. 4 Histological evaluation of PDX treated tumors. Representative 10× images and quantification of stained area of saline, CG and ChemGem treated tumors of (**A**) H&E and hematoxylin-stained area with H&E Color Deconvolution, (**B**) pan-cytokeratin, (**C**) vimentin (* p 0.0476), (**D**) Ki67 (* p 0.0176), and (**E**) cleaved caspase-3 (* p 0.0422) expression area with ImageJ Color Deconvolution H DAB using seven tumors per group, with three or four 10x images per tumor. Significance was determined using ANOVA and non-parametric Kruskal Wallis test

ChemGem compared to saline treated tumors (Fig. 4C). Furthermore, both ChemGem and CG treated tumors showed a decrease in proliferation rates (Fig. 4D), whereas ChemGem treated tumors also had a slight increase in tumor cell death, although this was not significant (Fig. 4E). Some tumors from saline group also displayed a high level of CC3 and necrotic areas, which can themselves have non-specific antibody binding.

In summary, ChemGem induced a significantly improved mouse survival (100%), decreased tumor growth with remaining lesions showing cystic behavior, and significantly smaller volumes.

Systemic gemcitabine resistance overcome with local treatment

In order to compare the effectivity and tolerability of ChemGem to systemic gemcitabine and to investigate potential immune dependent effects, we used the KPC3 syngeneic mouse model for PDAC (Fig. 5).

KPC3 tumors were remarkably resistant to systemic gemcitabine treatment (Fig. 5A-B), showing no effects of systemic gemcitabine on tumor growth. Intratumoral injections of ChemGem, however, showed a significant delay in tumor growth (Fig. 5D-F) and improved survival (Fig. 5G, ChemGem vs. CG p 0.0097), showcasing the important role of local drug delivery (Fig. 5H). Identification of the ChemoGell depot by the associated fluorescent signal, measured ex vivo, showed a slight increase in ChemGem treated tumors compared to CG and saline treated groups (Supp. Fig. 3B). This was likely because only ChemGem group received a T2 injection, in contrast to CG group, which received only T1 injection before reaching the experimental endpoint. No significant signal was detected in any organs, with the exception of the liver, where fluorescence signal could have been caused by cyclodextrin degradation. In addition, no difference in weight between treatment groups was observed (Fig. 5C, F). A ChemoGell depot was observed in end stage CG and ChemGem tumors (Fig. 5I).

Histological analysis was then performed on all tumors at the experimental endpoint. Data revealed a non-significant decrease in vimentin+ cells only in tumors treated with ChemGem, and no changes in pan-cytokeratin or Ki67 expression (Fig. 6A-C, E). Interestingly, a similar increasing trend in cleaved-caspase 3 expression was observed with ChemGem (Fig. 6D, E), although no difference was found compared to systemic treatment. Of note, well-defined necrotic cores were found only in mice bearing ChemGem treated tumors with the longest survival (Fig. 6F, median ChemGem 13 days vs. median gemcitabine 9 days). In

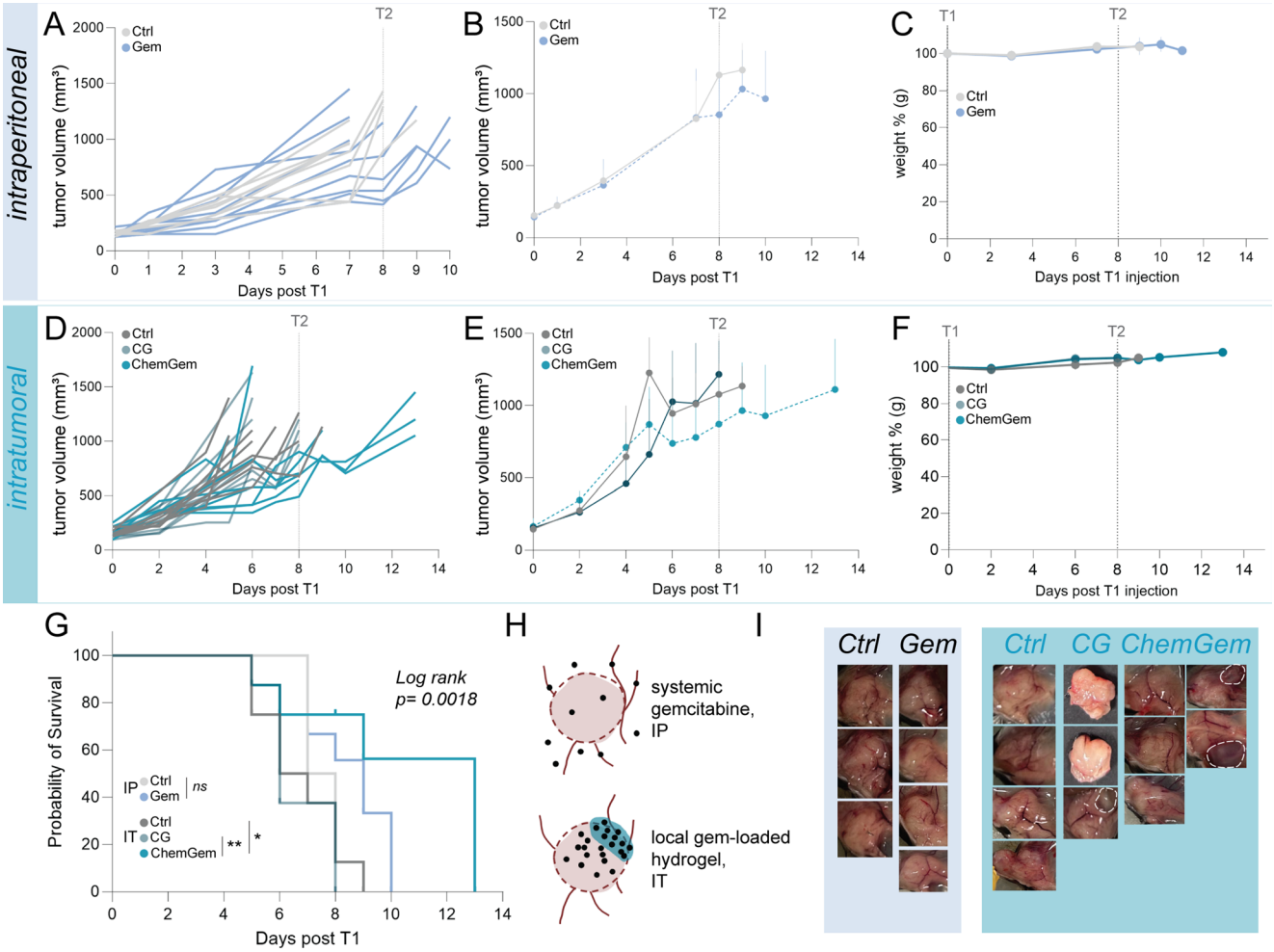

Fig. 5 Tumor growth reduction and improved survival of local delivery of gemcitabine-loaded hydrogel compared to non-effective systemic delivery in KPC3 murine pancreatic cancer model. **A** Individual tumor volume overtime of mice treated systemically with saline ($n=8$) and gemcitabine ($n=9$), measured by a calliper. First injection (T1) was performed at day 0, dotted line indicates second (T2) injections. **B** Tumor volume of systemically-treated mice measured overtime, plotted as cumulative mean ± standard deviation (SD), per treatment group. **C** Systemically-treated mice weight progression in percentage during the experiment, normalized to starting weight. **D** Individual tumor volume overtime of mice treated intratumorally with saline ($n=8$), ChemoGell (CG, $n=8$) and Gemcitabine-loaded CG (ChemGem, $n=8$), measured by a caliper. First injection (T1) was performed at day 0, dotted line indicates second (T2) injections. **E** Tumor volume of intratumorally-treated mice measured overtime, plotted as cumulative mean ± standard deviation (SD), per treatment group. **F** Systemically-treated mice weight progression in percentage during the experiment, normalized to starting weight. **G** Kaplan-Meier analysis of mice treated systemically with saline (median 7.5 days) and gemcitabine (median 9 days) (ns, 0.064), and intratumorally with saline (median 6.5 days), CG (median 6 days), and ChemGem (median 13 days) (Ctrl vs. ChemGem *, 0.0126; CG vs. ChemGem **, 0.0097) for a 2-week period. Overall significance was determined using a log rank test ($p=0.0018$). **H** Drawing to highlight difference between systemic delivery of gemcitabine and intratumoral delivery of gemcitabine-loaded hydrogel. **I**. Pictures showing hydrogel depots in CG and ChemGem tumors at HEP

addition, these necrotic cores were found to be in the proximity of the ChemGem depot in the tumor (Fig. 6G). These results may suggest that local ChemGem causes a rather quick cell-death effect compared to systemic gemcitabine due to the prolonged high drug exposure.

To evaluate gemcitabine-derived haematological side effects, we analyzed peripheral blood collected from the tail vein of these syngeneic KPC3-bearing mice 72 h after T1 injections. In both systemic and intratumoral treatment groups, reported gemcitabine-related side effects [20] such as neutropenia, thrombocytopenia and red blood cell count, were observed (Supp. Fig. 4). To further evaluate gemcitabine side effects, we performed an additional experiment with extended blood sampling using KPC3-luc2 model at i.e. 24 h, 72 h, 7 days and 14 days from each injection (Supp. Figs. 5–7). Interestingly, 24 h after T1 injection, hematocrit, hemoglobin and red blood cell count markers were significantly decreased only upon systemic gemcitabine, compared to respective controls (Supp. Fig. 6). These side effects, from both systemic and local delivery of gemcitabine, were reverted after 7 days (Supp. Fig. 7).

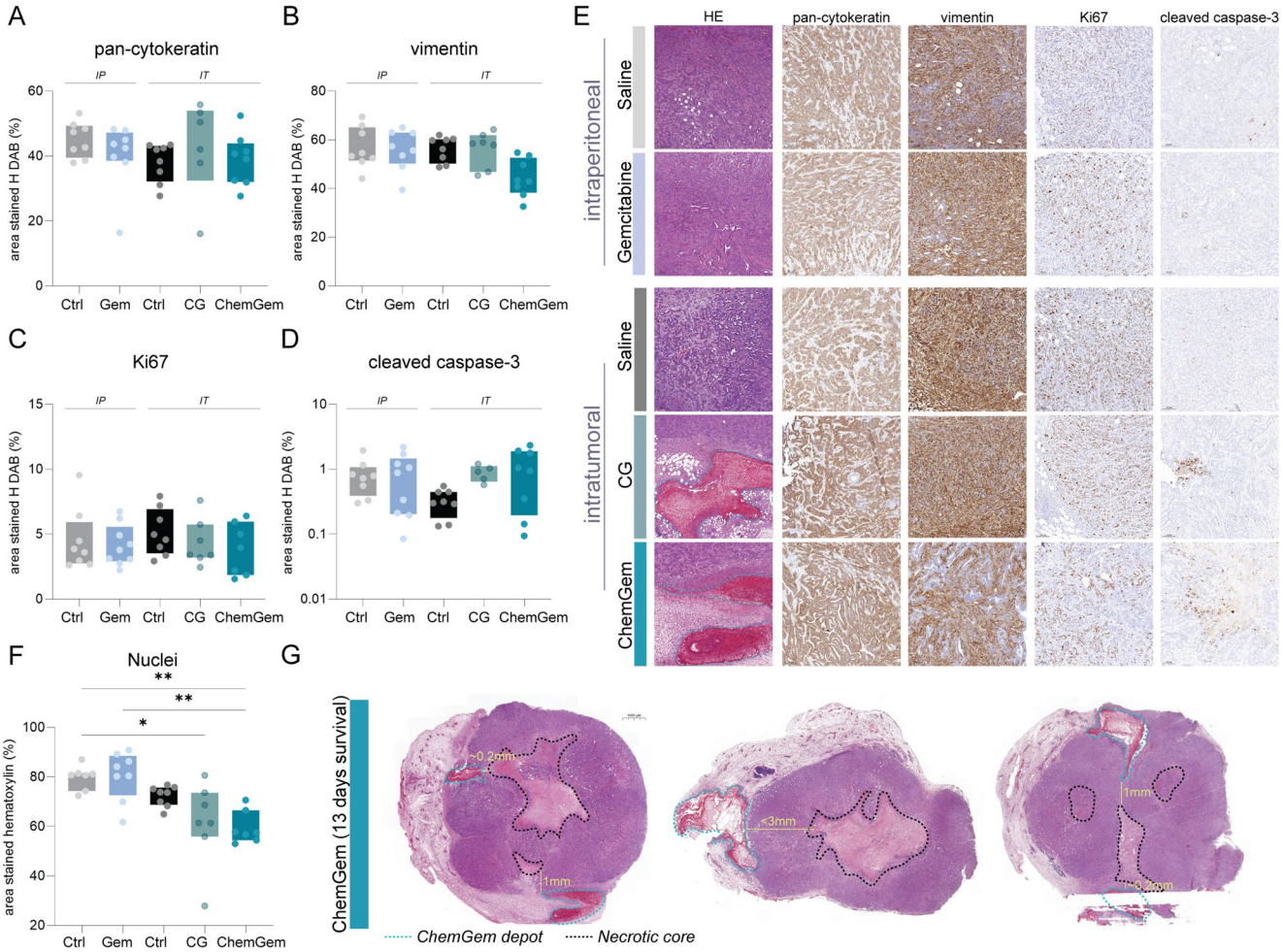

Fig. 6 Histological evaluation of syngeneic KPC3 treated tumors. **A-D.** Quantified (**A**) pan-cytokeratin, (**B**) vimentin, (**C**) Ki67, and (**D**) cleaved caspase-3 expression area with ImageJ Color Deconvolution H DAB using five to eight tumors per group, with at least three 10x quantified images per tumor. Significance was determined using ANOVA and non-parametric Kruskal Wallis test. **E** Representative 10× stainings of intraperitoneal (IP) saline and gemcitabine, and intratumoral (IT) saline, CG and ChemGem treated tumors. **F** Quantified hematoxylin via Color Deconvolution in ImageJ. Significance was determined using ANOVA and non-parametric Kruskal Wallis test (* p 0.0488, ** p 0.0034 and 0.0037, respectively). **G** H&E stainings of ChemGem treated tumors with a survival of 13 days. Necrotic cores depicted with dotted black lines, and ChemoGell depots depicted with blue dotted lines

Overall, intratumoral injections of gemcitabine-loaded thermoresponsive ChemoGell in KPC3 tumor-bearing mice were safe and tolerable. In contrast to the limited effectiveness of systemic gemcitabine, ChemGem effectively induced tumor cell death and significantly extended the survival of mice.

Stroma and immune cell dynamics upon ChemGem treatment and therapeutic implications

In order to investigate the potential role of the immune compartment on the effect of ChemGem, we evaluated peripheral lymphocytes and monocytes in peripheral blood samples. Peripheral lymphocytes were significantly increased upon systemic gemcitabine and ChemGem after 72 h of first injection in both KPC3 and KPC3-luc2 cohorts (Fig. 7A, B). Previously in PDAC patients treated with gemcitabine, it has been shown that activated naïve T cells are increased [21].

Seven days after first injection, peripheral lymphocytes were subsequently decreased in both systemic gemcitabine and ChemGem (Fig. 7C), however monocytes were significantly increased only in ChemGem treated tumors (Fig. 7D), in line with observations in PDAC patients treated with gemcitabine [21, 22]. Therefore, we further evaluated the histological expression of lymphocyte marker CD45 and macrophage marker F4/80 in KPC3 treated tumors. Both markers showed increased expression in ChemGem (Fig. 7E-H). In particular, CD45 + cells were increased within ChemGem tumors compared to the control groups, where CD45 cells remained mostly at the tumor barrier (Fig. 7E, F). This finding may be potentially associated with increased

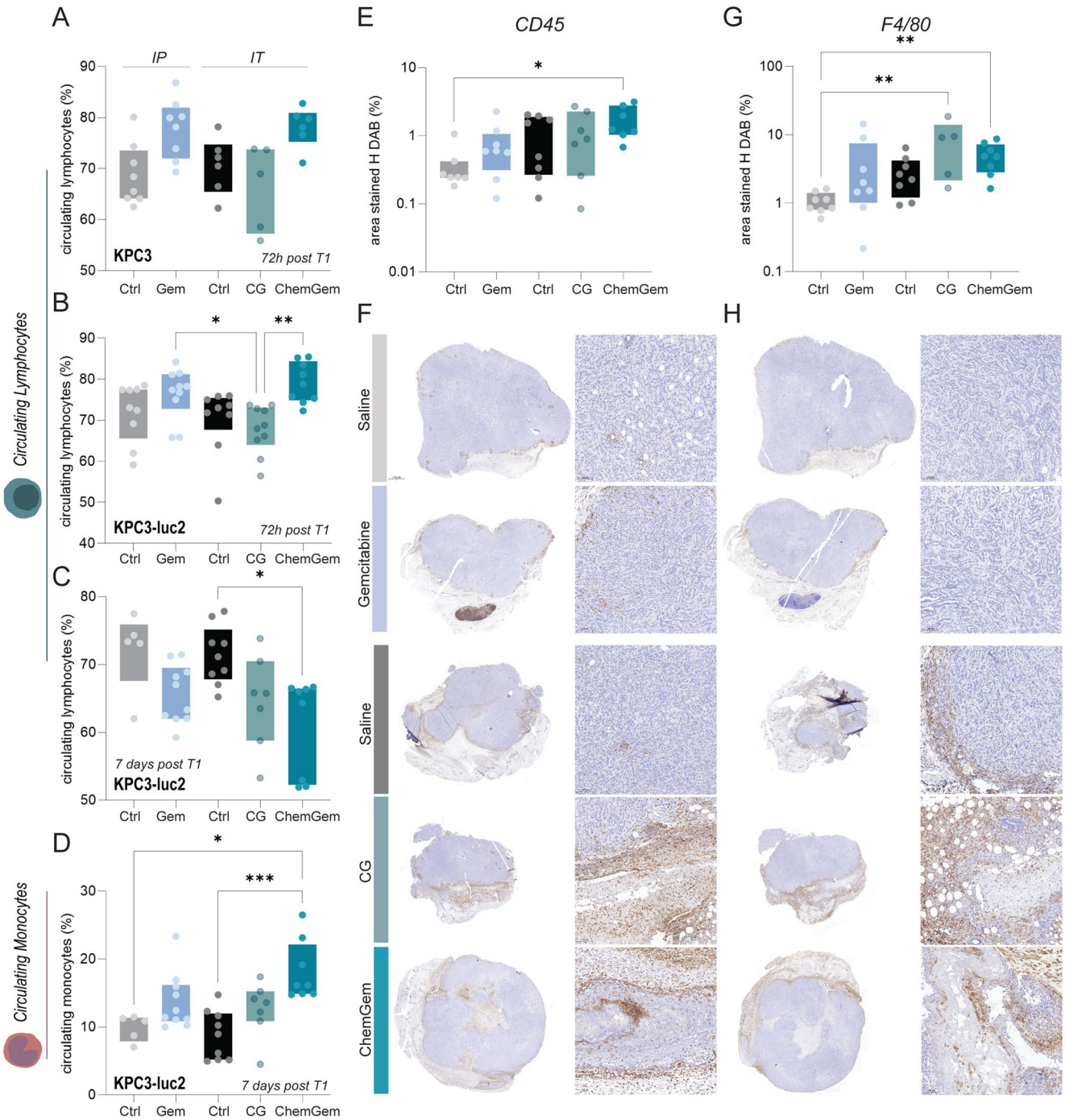

Fig. 7 Lymphocyte and monocyte dynamics upon ChemGem in syngeneic KPC3 treated tumors. **A** Peripheral blood circulating lymphocyte number after 72 h of first (T1) intraperitoneal (IP) and intratumoral (IT) injections. **B**, **C** Validation cohort of peripheral blood lymphocyte number after (**B**) 72 h and (**C**) 7 days (* p 0.0274) of T1 injections. **D** Peripheral blood monocyte number after 7 days (* p 0.0151, *** p 0.0009) of T1 injections. Significance was determined using ANOVA with multiple testing using non-parametric Kruskal Walis test. **E-H** Stained area quantification and representative images of (**E**), (**F**) Immune cell marker CD45 (* p 0.0281) and (**G**), (**H**) Macrophage marker F480 (** p 0.0052, ** p 0.0063, respectively), of the different treated tumors. Significance was determined using ANOVA with multiple testing using non-parametric Kruskal Walis test

gemcitabine tumor exposure. Of note, F4/80 + cells were also increased in empty CG-treated tumors (Fig. 7G, H).

Since hydrogel crosslinking and increased stiffness might promote fibrosis by the interplay of macrophages and fibroblasts [23], we further looked into both cell types within the ChemoGell depots of the KPC3 and PDX models. The cystic behaviour of PDX tumors treated with CG and ChemGem showed a significant increase in F4/80 macrophages (Supp. Fig. 8A, B). These were surrounding both the tumor islands and the ChemoGell depot, and also found within the depot. Similar findings were found in KPC3 tumors, where an interplay of fibroblasts (vimentin+), macrophages and lymphocytes was observed (Fig. 8A-D). To further understand the dynamics of the participating immune cells, we assessed the immune microenvironment and lymphoid activation in KPC3-luc2 tumors 7 days after intratumoral injections (Fig. 8E-L, Supp. Fig. 10, Supp. Fig. 11). Corroborating our results from end stage tumors, we noted an increase in infiltrating immune cells in the ChemGem treated tumors (Fig. 8E, F). On further characterizing the immune microenvironment, we observed an increased influx of NK-cells (p = 0.0259) and Monocytes (p = 0.0028) in ChemGem treated tumors compared to untreated controls (Fig. 8F-H). While there seems to be no change in macrophage influx at this timepoint (Fig. 8I), we note a polarization towards M0 macrophages (Fig. 8J), which we postulate derives from the increased monocyte infiltration in the treated tumors. Although ChemGem treatment led to no changes in CD8+, CD4 + or Treg infiltration into the tumors (Fig. 8K), we do observe a change in CD8 + T cell activation markers. These primarily involve an increase in KLRG-1 (ns), CXCR3 (ns), and CCR2 (p = 0.0045) expressing CD8 + T cells with a decrease in Naïve T cells (CD62L+, CD44-) (ns) and PD-1 expressing CD8 + T cells (p = 0.0024) (Fig. 8L, Supp. Fig. 11) compared to untreated controls.

Interestingly, ChemoGell depots displayed infiltration/presence of activated αSMA+ fibroblasts and M1 iNOS+ macrophages (Fig. 8M), as well as cytotoxic T cells (CD8+) nearby macrophages (F4/80+) (Fig. 8N) at the end stage of the tumors. Furthermore, the ChemGem treated mice with longest survival displayed high levels of CD8 + T cells within the necrotic areas, as well as increased F4/80 + macrophages in the tumor border (Supp. Fig. 9).

Altogether, we demonstrated the advantages of using localized delivery of ChemGem, showing a marked benefit compared to a systemic Gem treatment in KPC3-luc2 tumors and a 100% survival in the PDX model. The strength of ChemGem also derives from its capacity to modulate the TME. In brief, we showed that ChemGem can drive an immune response within the tumor, leading to an early systemic and local increase in monocytes which seem to differentiate into M0-Macrophages around 7 days into treatment. These Macrophages further polarize into an M1 phenotype in the proximity of the ChemGem depot at later stages, consistent with a temporal shift from initial monocyte recruitment and M0 differentiation to M1 polarization driven by sustained local drug release and/or matrix degradation. Moreover, we illustrate an influx of NK-cells and activated T-cells within the treated tumors showing an opportunity for further research co-stimulating the immune infiltrate (Fig. 8N). Finding novel ways to inactivate infiltrating CAFs, while exploiting the increased Immune infiltration might therefore be key in improving treatment responses in PDAC.

Discussion

Gemcitabine is a widely used chemotherapeutic agent for the treatment of PDAC. However, achieving sufficient intratumoral concentrations of gemcitabine remains a significant challenge. This is mainly due to the high expression of drug efflux pumps in this tumor type, together with the presence of a highly dense and fibrotic extracellular matrix, which poses a significant physical barrier to drug penetration [24]. Intratumoral delivery platforms aim to bypass these mechanisms and expose the tumor to high concentrations of chemotherapy, while sparing systemic toxicity [25]. ChemoGell has been uniquely formulated to achieve this function by possessing highly injectable properties and a 2-phase crosslinking mechanism providing high site retention and stability. In practice variation in needle and tumor positioning may prolong procedural workflows, holding ChemoGell for longer than the 3 min incubation tested in this study. Therefore, for thermoresponsive systems intended for endoscopic delivery, stress testing of formulation residence times, at body temperature need to be performed and will inform a timeframe for clinicians to complete injection procedures.

ChemoGell is formulated with clinically understood components that also provide capacity for hydrophilic and hydrophobic chemotherapy drugs; positioning the platform for an accelerated clinical translative pathway. Here, by encapsulating gemcitabine in ChemoGell, we have been able to show these properties, and demonstrate an increase in chemotherapy efficacy to the non-effective systemic approach. The inclusion of gemcitabine HCl into ChemoGell did alter the physical characteristics of the hydrogel platform. However, the functional properties for injectable delivery, thermoresponsive gelation and in situ retention were all demonstrated. Moreover, in vitro disintegration testing and gemcitabine release was slowed and delayed under acidic conditions relevant to the PDAC tumor microenvironment [26]. This in vitro data also indicated the pH range that ChemGem could reliably initiate secondary

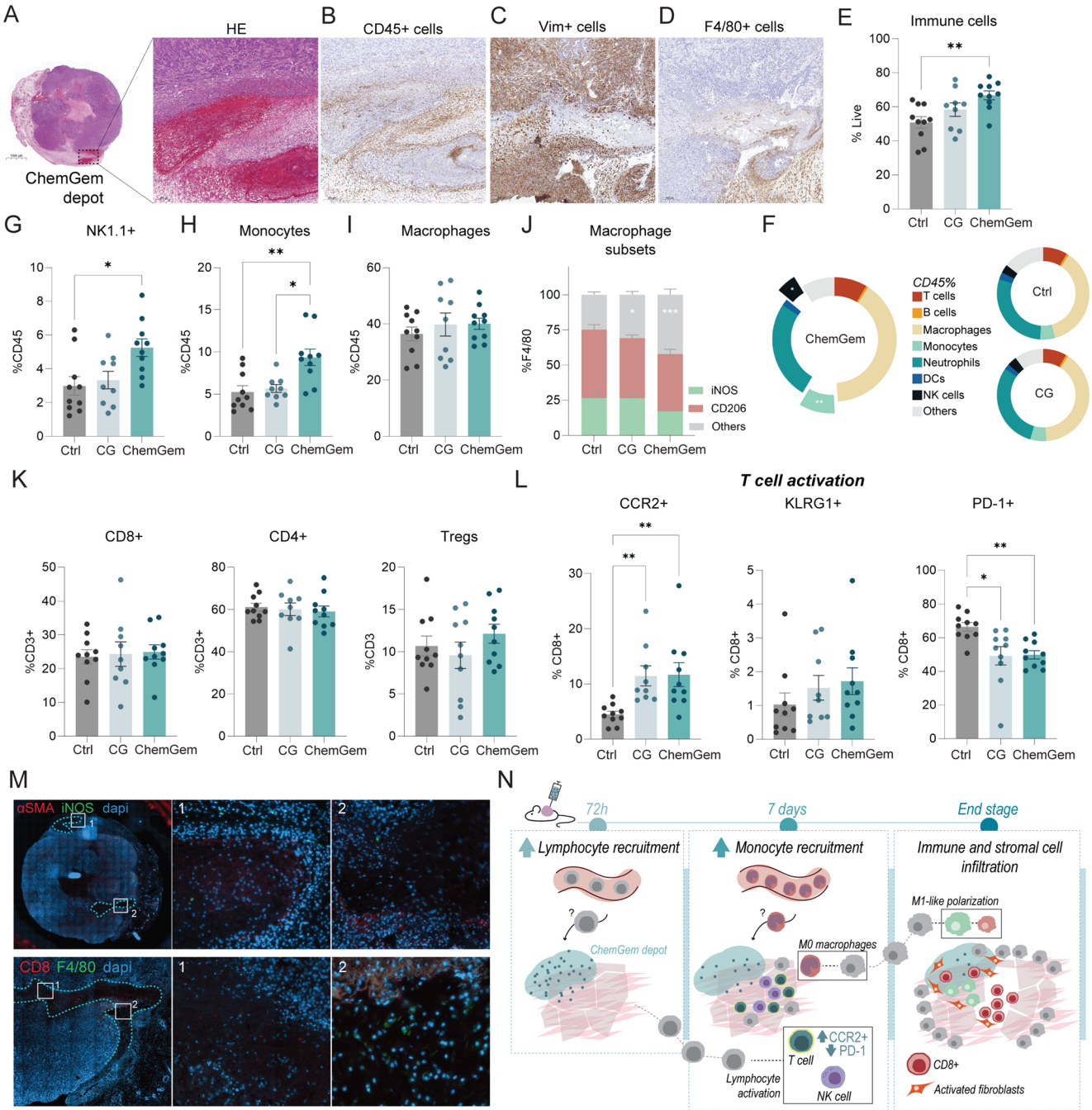

Fig. 8 Immunomodulatory effects of ChemGem depot in KPC3 pancreatic tumors. **A** HE, (**B**) Immune cell marker CD45, **(C)** Stromal cell marker vimentin and (**D**) Macrophage marker F4/80 IHC staining of a ChemGem treated KPC3 tumor. (**E-L**) Immunomodulatory differences between saline (Ctrl), CG, and ChemGem treated KPC3-luc2 tumors ($n=10$/group), based on (**E**) Immune cells (%) gated from total of Live cells (See Supp. Fig. 10). **F** Analysis of Immune cells populations from CD45+cells consisting of T cells (CD3+) NK cells (NK1.1+), B cells (CD19+), Neutrophils (CD11b+,Ly6G+), Macrophages (CD11b+,F4/80+), DCs (CD11b-,CD11c+) and Monocytes (CD11b+,Ly6G-,Ly6Chigh) Frequency of (**G**) NK1.1+cells, (**H**) Monocytes (CD11b+,Ly6G-,Ly6Chigh), **(I)** Macrophages (CD11b+,Ly6G-,F4/80+) from CD45+cells in KPC3-luc2 tumors, (**J**) Stacked barplot showing frequency of M1 (iNOS+CD206-), M2 (iNOS-,CD206+) and M0 (iNOS-,CD206-) macrophages. (**K**) Frequency of CD8+, CD4+and Treg T cells from CD3+cells (**L**) CD8+activation markers CCR2+, KLRG1+and PD-1+ (Related to Supp. Fig. 11). **M** Activated fibroblasts (αSMA+) and M1-like macrophages (iNOS+), macrophages (F4/80+) and cytotoxic T cells (CD8a+) in *ChemoGell* depot area of a ChemGem treated KPC3 tumor, via IF staining. Cyclodextrin-FITC contained in *ChemoGell* also emitted fluorescence as depicted in E1 and F2 images. **N** Schematic drawing of immunomodulatory effects in ChemGem

cross-linkage for site retention for local release. These observations suggested a loading of 2%w/w of gemcitabine HCl was feasibly deliverable for subsequent in vivo study. Moreover, this loading concentration enabled the equivalent IP injection dose (50 mg/kg) to be applied entirely within the tumor region as part of the in vivo study design. This localized delivery did not seem to have any apparent additional side effects to the systemic gemcitabine-related adverse effects on the mice. Moreover, ChemoGell retention at tumor site was proven for at least 13 days in the syngeneic model, and 53 days in the PDX model, the longest period recorded for the ChemoGell platform [12].

While we only observed injection site retention, tolerability and treatment efficacy, the subsequent breakdown and excretion of gemcitabine and the platform's excipients still require a direct in vivo pharmacokinetic study, capturing the intratumoral aspect. With that said, the potential safety of the excipients as an intratumoral formulation is supported by their generally well characterised clearance profiles. Specifically, P407 and HP-β-CD are expected to clear mainly by release from the depot followed by renal excretion, while chitosan undergoes gradual local biodegradation prior to elimination [27–30]. Genipin has the least clinical use and safety data is limited to one clinical trial using genipin injected intravertebrally that concluded it was a safe intervention. Human pharmacokinetic data for genipin is currently not available, however animal studies show rapid metabolism of genipin and excretion via renal and hepatobiliary routes [31, 32]. In the case of a local intratumoral depot, the clearance pathways reported in the literature may not directly reflect the intended route of administration, as most available data are not derived from local depot formulations. Rather, systemic exposure would probably depend on the gradual breakdown of the depot and subsequent release into the circulation, suggesting a low risk of prolonged healthy tissue exposure or significant systemic toxicity. Given that empty ChemoGell showed inherent anti-tumor and immunomodulatory properties, it remains challenging to fully decouple drug-induced immunogenic cell death from matrix-induced inflammation, and future mechanistic studies may include a genipin-free hydrogel control.

Our findings underscore the potential of ChemGem delivery intratumorally as a promising therapeutic strategy for pancreatic adenocarcinoma. The in vitro and ex vivo results demonstrated substantial induction of cell death in patient-derived organoids and explants of resected PDAC tissue. The safety, tolerability and efficacy of ChemGem was further confirmed in vivo using PDX models, where it significantly reduced tumor growth, induced tumor cell death, and increased survival to 100%. In addition, in the aggressive and mutant *p53* and *K-ras* KPC3 murine model, ChemGem achieved increased tumor control compared to the ineffective systemic gemcitabine treatment.

Furthermore, we showed that an immunologically "cold" and aggressive PDAC tumor responded better to the localized gemcitabine-loaded ChemoGell compared to systemic gemcitabine. ChemoGell depots were found to be infiltrated with activated fibroblasts, M1-type macrophages and cytotoxic T cells, indicating that ChemoGell might have an immune-modulatory effect in these tumors. KPC3-tumor bearing mice treated with ChemGem displayed an increased number of circulating monocytes in blood after 7 days of treatment. Upon interrogating tumor infiltrating immune cells, we observed a significant increase in NK-cell and monocyte infiltration, coupled with the increase in activated CD8 + T cells in the tumor. These findings are in line with previously described immunomodulatory abilities of gemcitabine in PDAC patients [21, 22, 33], which opens the door to synergy with immunotherapeutic strategies, especially targeting co-stimulatory mechanisms of T cells [34, 35]. Studies have shown hydrogel crosslinking is able to influence macrophages, fibroblasts, and their interactions during wound healing [23]. A recent in vivo study in PDAC using a peptide hydrogel successfully transformed an immunologically "cold" tumor into a "hot" tumor by activating dendritic cell maturation, recruiting tumor-infiltrating lymphocytes, and reducing hypoxia within the tumor microenvironment [36]. Similarly, other studies using a drug-loaded hydrogel have shown immunogenic cell death, increased macrophage and CD8 T cell infiltration [37, 38]. Likewise, we also observed CD45 and CD8 T cell infiltration surrounding ChemoGell depots and in necrotic cores of ChemGem tumors, potentially suggesting a less immunosuppressive phenotype [39].

Empty ChemoGell showed a decrease in organoid viability, and a slight tumor growth delay in our PDX model, in line with a previous study where the ChemoGell formulation demonstrated chemo-ablative properties [12]. This is thought to be possibly due to genipin, contained in ChemoGell, which has been used as an anticancer agent in preclinical models on multiple cancer types, including pancreatic and gastric cancer [40], and/or due to poloxamer polymer, which has also been shown to increase therapeutic efficacy of injectables [41].

In the clinical setting, intratumoral injections offer a promising approach for treating solid tumors, which account for approximately 90% of all cancers and are often localized or regionally confined. However, intratumoral injections to distant organ site are reliant on the use of minimally invasive approaches, which often require high gauge needles and long catheters. Therefore, injectability is an important consideration. Prior to sol-gel transition, ChemoGell is a shear-thinning polymer solution, which facilitates syringe loading

and needle injection. The low viscosity of the formulation was shown to allow extrusion via a range of clinically relevant needles that could apply ChemoGell. Additionally, the exposure of the delivery devices to a heated environment (37 °C) still allowed for feasible injection, showing that heat transfer to the needle or catheter during the positioning of the needle to the tumor site should not impede the intratumoral delivery of the formulation. Further assessment of injectability in patients is guaranteed.

Specifically in the treatment of PDAC, access to tumors in the head of the pancreas can be achieved either using endoscopic ultrasound-guided fine-needle injection (EUS-FNI) or percutaneous injection. EUS-FNI is routinely performed as a diagnostic procedure in pancreatic cancer patients [42] and EUS-guided injectable therapies have shown to be safe and have potential efficacy in the treatment of PDAC [43]. In our preclinical study, we administered only two single-site injections with 8 days in between, but recent studies have suggested that multisite injections could be more effective than single-site injection [44]. For patient tumors of 4–5 cm size, it is likely that multiple injections are required to achieve adequate hydrogel spread and maximize effective chemo exposure throughout the tumor. Hence, future studies may evaluate the efficacy of ChemoGell using multiple site injections.

Clinically, localized gemcitabine-loaded ChemoGell could be primarily beneficial in the neoadjuvant setting for borderline resectable PDAC for tumor debulking, and in the palliative setting, for local disease control in locally advanced tumors (Fig. 9). Thus, patients with local advanced disease that are not eligible for surgical resection, or that do not respond to neoadjuvant chemotherapy (> 30% PDAC patients) could potentially benefit from this localized strategy [45]. Particularly for the treatment of locally advanced PDAC, intratumoral delivery of therapy has shown promising results. For instance, paclitaxel microparticles combined with the standard of care have demonstrated an enhanced immune response, improved disease control rate, increased resection rate, and extended survival [46]. In a phase I trial, the use of the intratumoral HF10 oncolytic virus alongside systemic erlotinib and gemcitabine also showed potential for locally advanced pancreatic cancer [47]. Furthermore, for patients where FOLFIRINOX is not recommended due to frailty or high toxicity [48, 49], further studies are planned to explore the potential of the combination of gemcitabine-loaded ChemoGell with other treatments such as systemic nab-paclitaxel, or radiotherapy.

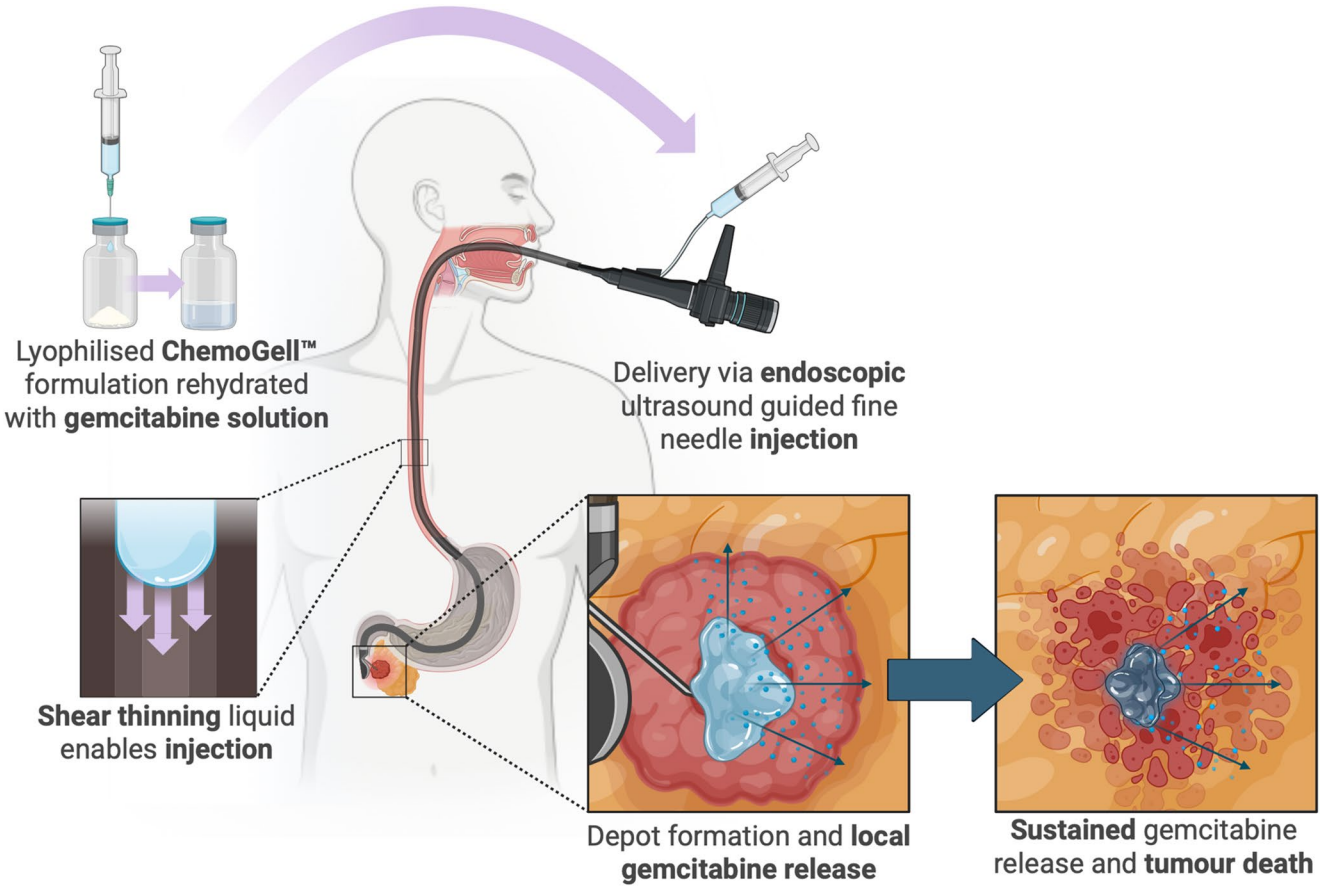

Fig. 9 The proposed clinical application of the developed *ChemoGell* platform

Conclusion

Overall, our findings show that localized ChemGem injections in preclinical PDAC models have a significant effect in reducing tumor growth and improving survival. This is further accompanied by a modulation of the stroma, driving an influx of active stromal and immune populations. This positions ChemGem as a potential new intratumoral hydrogel therapy that could overcome the current limitations of local delivery of conventional systemic chemotherapy, offering a more effective, sustained and localized therapeutic option for PDAC patients, particularly those with borderline resectable or locally advance tumors.

Methods

Preparation of blank ChemoGell and gemcitabine loaded ChemoGell

The ChemoGell (OncoLize BV) thermoresponsive polymer solution was generated from a lyophilised blend of Poloxamer 407 (P407) (BASF, Ludwigshafen, Germany), hydroxypropyl-beta-cyclodextrin (HP-β-CD) (Cyclodex, Alachua FL, USA), chitosan (Heppe Medical Chitosan+, Halle, Germany) and genipin (TGY Bio, Xi An, Shaanxi, China), as previously described [11] (patent number US20230126053). For in situ fluorescent imaging a small proportion of HP-β-CD was replaced with a FITC conjugated cyclodextrin (HP-β-CD, CycloLab Ltd., Budapest, Hungary). The polymer solution was aliquoted into vials, snap frozen in liquid nitrogen and then lyophilized at 0.1mbar and − 60 °C condenser temperature for 18 h. Lyophilisate was sterilised using ethylene oxide gas exposure with a cycle and purge lasting 12 h. Within 5 days prior to intratumoral injections, lyophilised ChemoGell was aseptically reconstituted using sterile endotoxin free water or a sterile filtered (0.22 µm) aqueous solution of gemcitabine HCl (FluoroChem, Cork, Ireland). The final concentration of gemcitabine HCl being 2% w/w. Samples were left to hydrate overnight at 4 °C with mixing.

Table 1 Clinically relevant needles used for injection force testing

Needle Gauge	Working Length (cm)	Needle Name	Manufacturer	Abbreviation
25G	1.5	Microlance needles	BD	25G
20G	10	Chiba biopsy needles	Wellgo	20G Biopsy
19G	137.5–141.5	Endoscopic ultrasound FNA system	Micro Tech	19G FNA

Rheological analysis of ChemoGell

Material properties of CG and ChemGem formulations were assessed using oscillatory and flow measurements on a Discovery HR1 rheometer (TA instruments, Delaware, USA) with a cone/plate geometry (40 mm diameter, 4° cone angle). Samples were placed onto the temperature-controlled Peltier plate, pre-equilibrated to 20 °C and covered with a solvent trap during testing. Sol-gel transition temperature was determined using an oscillatory test at 1 Hz, applying 5 Pa of stress at 1 °C increments from 20 to 40 °C. Gelated stiffness was determined by the same oscillatory test (1 Hz and 5 Pa of stress) over 30 min fixed at 37 °C. Shear thinning properties were assessed at 21 °C under increasing shearing rate from 1 to 500 s^{-1}.

Injection force testing of ChemoGell

Injectability testing was conducted using a Zwick Universal Testing Machine (ZwickRoell Z2005) equipped with a 50 N load cell. Luer-Lock 1 ml syringes were filled with ChemoGell and fitted on a needle holder attached to two retort stands. The entire 1 ml contents were expelled at a rate of 1 mm/s, at room temperature and the maximum force required was recorded. Three different types of needles were tested (Table 1):

In vitro ChemoGell disintegration and gemcitabine release from ChemGem

0.5 ml depots of CG-Gem and CG were gelated at 37 °C at the bottom of a pre-weighed 2 ml Eppendorf tube before adding 1 ml of either PBS (pH 7.4), Tris buffer (Trizma HCl and Trizma base, pH 8.5) or acetate buffer (sodium acetate, acetic acid pH adjusted with NaOH to pH 5.5). At predetermined timepoints, the supernatant was collected off and excess surface residue was removed by spotting a KimTech wipe. Each tube was then weighed before returning to the 37 °C water bath and reintroducing 1 ml of fresh prewarmed buffer.

Gemcitabine release into the supernatant was quantified using reverse phase-HPLC. Completed using an Eclipse Plus C18 Column (4.6 mm × 150 mm, (5 µm), Agilent), mobile phase 95% water 5% acetonitrile, 1 ml/min flow rate, 10 µl injection volume and 25 °C column temp. Detection of gemcitabine was captured using a UV poly-diode array lamp with peak analysis at 269 nm.

Cell lines, organoids and explants

The primary KPC tumor cell with mutant *TP53* and *KRAS* derived from a female C57BL/6 mouse [50] (KPC3, RRID:

CVCL_A9ZK) was used for the syngeneic in vivo experiments. The KPC3-luc2 murine pancreatic cancer cell line expressing firefly luc2 [51] was also used as an additional blood sampling cohort. Cell lines were cultured as adherent monolayers in IMDM supplemented with 8% v/v fetal bovine serum (FBS) and 1% v/v Pen/Strep solution, and maintained at 37 °C and 5% CO_2. Cell lines were validated by short tandem repeat (STR) profiling (IDEXX BioAnalytics, Ludwigsburg, Germany) and mycoplasma tests were performed on a monthly basis.

Patient-derived organoids Pac12 and Pac09 were derived from an endoscopic-ultrasound (EUS)-guided fine-needle biopsy, and Pac42 and Pac60 were derived from a surgical resection specimen, from four different human PDAC patients. Pac12, Pac09, and Pac42 were treatment naïve patients, and Pac60 patient was treated with neoadjuvant FOLFIRINOX. Patient-derived explants Pac73 (cancer tissue) and Pan73 (normal-adjacent tissue) were derived from a surgically resected human pancreatic cancer sample. Tissues were used in accordance with the Code of Conduct for Responsible Use of human tissues, and after written informed consent was obtained. Approval for this study was obtained from the biobank committee as part of the medical ethics committee of the Leiden University Medical center and registered under protocol RP 24.004. Organoids were expanded according to previously established procedures [52, 53]. In brief, organoids were embedded in growth factor reduced Matrigel (GFR-Matrigel, phenol red free, Corning) and cultured in complete medium: AdDMEM/F12 medium supplemented with 5mM HEPES (GIBCO), Glutamine/Glutamax (200 nM 100x, Invitrogen), 1% penicillin/streptomycin (Thermo Fisher Scientific), 1x B27 supplement (Invitrogen), 1 mg/ml Primocin (InvivoGen), 1.5 mM N-acetyl-L-cysteine (Sigma), Wnt-3a Recombinant Protein 0.5 nM (PeproTech), recombinant R-Spondin 3 100 ng/mL (Peprotech), recombinant Noggin 100 ng/mL (Peprotech), 50 ng/mL epidermal growth factor (EGF; Peprotech), 10 nM Gastrin (Sigma), recombinant FGF10A 100 ng/mL (Peprotech), 10 mM Nicotinamide (Sigma), and 0.5 mM A83-01 Alk5 inhibitor (Selleckhem).

Organoid treatment

ChemoGell injections into the organoid dome were tested in vitro, in four different patient-derived organoids. In brief, the day prior to treatment, organoids were dissociated using cold AdDMEM, centrifuged at 1200 rpm for 5 min at 4 °C, before removing the supernatant and Matrigel. Then, fresh cold medium was added and organoids were mechanically disrupted into fragments by the use of a needle and a syringe. After centrifuging, the pellet of organoid fragments was resuspended in Matrigel and seeded as 50 µl domes in 24 well plates. Domes were solidified by incubating for 6 min at 37 °C, before 500 µl of warm, complete organoid medium was added. The day after, organoids were treated i.e. non-injected, PBS-, CG- and ChemGem injected. Intradome injections were performed by injecting 10 µl of each treatment, perpendicular to the dome surface using insulin needles. Mechanical/shear stress damage to the organoids was excluded using a PBS injection control and an empty ChemoGell control. Intradome treatment solutions were all kept cold for the procedure. After 3 days of treatment, media was refreshed. At day 5, organoid cell death and viability were evaluated first by the use of propidium iodide (PI, Cat. #P4170, final concentration 5 µg/ml) and Hoechst 33,342 stain (Cell Signaling Technology Cat. #4082, RRID: AB_10626776), and subsequently by Cell Titer Glo 3D viability assay (Promega). All bright field, fluorescence and luminescence images and measurements were captured using a Cytation 5 Cell Imaging Multi-Mode Reader (BioTek Instruments, Inc, Winooski, VT).

Explant treatment

Tumor and normal resected tissue samples were sliced into 0.5–1 × 1 cm pieces. The pieces were allocated into individual wells of a 24-well plate containing warm Advanced DMEM. Injections were prepared on ice using insulin needles. Each tissue piece was injected perpendicularly to the tissue with a total volume of 10 µl of PBS, CG and ChemGem, followed by incubation at 37 °C. After 24 h, tissue samples were fixed in 4% formalin and paraffin embedded for subsequent tissue stainings.

Animal experiments

All animal experiments were performed in accordance with the ARRIVE guidelines, and with the Dutch Act on Animal Experimentation and EU Directive 2010/63/EU, and approved by the institutional Animal Welfare Body of Leiden University Medical Center (the Netherlands), and carried out under project license AVD11600202216549 issued by the competent authority on animal experiments in the Netherlands (CCD: Centrale Commissie Dierproeven).

Immunodeficient female xenograft NSGs (NOD, Cg-Prkdc scid Il2rg tm1 Wjl/SzJ; 6–8 weeks old, own breeding) were used to evaluate tumor growth. Mice received a subcutaneous implant of an established PDAC patient-derived xenograft in the right flank under analgesia (Buprenorphine, Temgesic) and inhalation anaesthesia (isoflurane 2–3%). Once tumors were palpable (~4–5 week post implantation), tumor volume was monitored twice per week by the use of a calliper. A total of 21 successfully engrafted mice were included in the study, divided into 3 groups, with 7 mice per

group and a statistical power of 0.8163. Upon reaching the humane endpoint (HEP: tumor volume $\geq 1500mm^3$, tumor ulceration, extreme weight loss and/or abnormal behaviour) or max. 112 days post inoculation, mice were euthanized through CO_2.

For the KPC3 experiments, immunocompetent female C57BL/6J mice (RRID: IMSR_JAX:000664) were purchased from Charles River Laboratories. For the formation of tumors, a total of 10^5 KPC3 cells were injected subcutaneously into the right flank of 6–12-week-old C57BL/6J mice with a total volume of 100 µl PBS/0,1% BSA. Once tumors were palpable (~ 11–14 days post injection), tumor volume was monitored three times per week by the use of a calliper. Upon reaching the HEP (tumor volume ≥ 1000mm3, tumor ulceration, extreme weight loss and/or abnormal behavior), mice were euthanized through CO_2. A total of 41 tumor-bearing mice were included in the experiment, divided into five groups, with 8–9 mice per group, with a statistical power of 0.8724.

To further evaluate the haematological/immune effect of intratumoral injections, we made use of a second cohort with female Albino B6 (B6(Cg)-Tyr < c-2 J>/Lumc (C57/Bl6 albino). For the formation of tumors, a total of 10^5 KPC3-luc2 cells were injected subcutaneously into the right flank of 6–12-week-old Albino B6 mice with a total volume of 100 µl PBS/0,1% BSA. Once tumors were palpable (19 days post injection), tumor volume was monitored three times per week by the use of a calliper. Upon reaching the humane endpoint (HEP, ≥ 1500mm3, tumor ulceration, extreme weight loss and/or abnormal behavior), mice were euthanized through CO_2. A total of 27 tumor-bearing mice were included in the experiment, divided into three groups, with 9 mice per group, with a statistical power of 0.9548.

Additionally, to functionally assess and characterize the immune infiltrate into the treated tumors, a total of 10^5 KPC3-luc2 cells were injected subcutaneously into the right flank of 6–12-week-old C57BL/6J mice with a total volume of 100 µl PBS/0,1% BSA. Tumor volume was then monitored as previously described.

For KPC3, KPC3-luc2 and PDX mice survival experiments, and to ensure that all treatment groups had similar tumor volume at the start of the treatment, mice were treated once tumors reached $125mm^3 \pm 25mm^3$. For both systemic and local treatments, two injections were performed at day 0 and day 8 from the start of treatment under anaesthesia. For the KPC3-luc2 mice experiment interrogating the immune effects, mice were treated once tumors reached $125mm^3 \pm 25mm^3$ and tumors were collected after 7 days of treatment.

Systemic treatments consisted of intraperitoneal injections (100 µl) of saline or gemcitabine HCl dosed at 50 mg/kg. Local treatments consisted of intratumoral injections (50 µl) of saline, empty ChemoGell or Gemcitabine-loaded ChemoGell. equal dose of gemcitabine HCl was administered in both intratumoral and intraperitoneal injections. At the end of the experiment, tumors and organs (liver, spleen, kidneys and heart) were collected, fixed in 4% formalin and embedded in paraffin for further experiments. Mice displaying tumor ulceration bearing tumors $\leq 500mm^3$ were excluded from the analyses.

Fluorescence in vivo and ex vivo imaging

To evaluate the presence of ChemoGell depot, the FITC signal of cyclodextrin (ex. 465, em. 530) contained in ChemoGell, was measured under anesthesia 2 h after first injection and 2 h before second injection in vivo. Additionally, fluorescent signals were measured from ex vivo tumors and organs after euthanasia. Signals were captured using the Lago X instrument (Spectral Instruments Imaging, Bruker). Subsequently, tumors and organs were fixed in 4% paraformaldehyde and embedded in paraffin for further analysis. To reduce fluorescence background signal, non-fluorescent 2016 Teklad global 16% protein feed (Inotiv) was given to all mice for the duration of the study.

Blood sampling and analyses in vivo

To assess systemic toxicity, peripheral blood of C57BL/6J mice bearing KPC3 tumors was collected via tail vein puncture using heparin coated tubes (max. 25 µl/sample) 72 h after the first injections, under a warming lamp. A total of 20 µl were transferred to solvent-prefilled tubes, and then analyzed using the Urit V5 smart hematology analyzer. Haematological markers such as red blood cell count (RBC), white blood cell count (WBC), haematocrit (HCT) and platelet count were included. Peripheral blood of the second cohort of C57/Bl6 albino mice bearing KPC3-luc2 tumors was collected as described after 24 h, 72 h, 7 days and 14 days of both intratumoral injections.

Tumor and organ staining

Histochemical stainings were performed on 4% formalin fixed, paraffin embedded tumor and organ 4-µm sections. Mounted slides were deparaffinized, rehydrated, and stained for haematoxylin and eosin (HE). To evaluate ChemoGell depot in tumors, Safranin/O Fast-green staining [54] was used to stain the chitosan, contained in ChemoGell.

For immunohistochemical (IHC) stainings, formalin-fixed, paraffin embedded tissue 4 µm were deparaffinized and an additional blocking step of 0.3% hydrogen peroxidase (Merck) in methanol was performed for 20 min. Once rehydrated, antigen retrieval was performed by boiling in

0.01 mol/l sodium citrate (pH 6.0). Slides then were washed and incubated with primary antibodies diluted in 1% PBS/bovine serum albumin (BSA) overnight. Primary antibodies used were: anti-Pan-cytokeratin (1:3200, clone PCK26, Sigma), anti-Vimentin (1:400, clone d21h3, Cat #5741s, Cell Signaling Technology), anti-Ki67 monoclonal antibody (1:200, SP6, Cat #ab16667, Abcam), anti-Cleaved Caspase-3 polyclonal antibody (1:200, Asp175, Cat #9661, Cell Signaling Technology), anti-F4/80 (1:800, clone BM8, Cat #14-4801-82, eBioscience) and anti-CD45 (1:200, Cat #30-F11, eBioscience). Antibodies were diluted in 1% PBS/BSA and incubated at the recommended temperature overnight. Then, samples were incubated for 30 min at RT with goat anti-rabbit (Ab6720, Abcam) and goat anti-mouse (Ab6788, Abcam) biotinylated secondary antibodies followed by incubation with avidin biotin complex (VECTASTAIN® Elite® ABC HRP Kit; Vector Laboratories). Peroxidase activity was detected using the 2-component liquid DAB+ system (Agilent) according to the manufacturer's instructions for 5 min. Slides were counterstained in haematoxylin (Sigma Aldrich), dehydrated, and mounted using Entellan (Sigma Aldrich). Control sections were processed in parallel, but without incubation with primary antibody. No labelling was observed in the negative control slides.

All HE and IHC slides were scanned with the Pannoramic 250 slide scanner (version 1.23; 3DHISTECH, Ltd, Budapest, Hungary). Images were obtained using Caseviewer (version 2.4; 3DHISTECH, Ltd).

For immunofluorescent (IF) stainings, the spectral IF panels used were αSMA, iNOS, and CD8α, F4/80, and DAPI. Tumor slides were then incubated with anti-mouse αSMA monoclonal (61001, Progen) and rabbit anti-mouse iNOS (PA3-030 A, ThermoFisher), or rat anti-mouse F4/80 monoclonal (clone BM8, Cat #14-4801-82, eBioscience) and rabbit anti-mouse CD8α monoclonal (D4W2Z) antibodies diluted in 1% PBS/BSA at the recommended temperature overnight. Slides were then washed in PBS and incubated with donkey anti-rat AF488 (A21208, Invitrogen) and donkey anti-rabbit AF555 (A31572, Invitrogen), or donkey anti-rabbit IgG AF488 (A21206, Invitrogen) and donkey anti-mouse AF555 (A31570, Invitrogen) secondary antibody diluted in PBS for 30 min at room temperature in the dark. Nuclear counterstaining was performed by mounting with ProLong DAPI (P36931, ThermoFisher) at room temperature. All IF images were obtained with the Widefield Leica DM6B1 microscope (Leica Microsystems).

Cell preparation for flow cytometry

Tumors were minced in small pieces and additionally incubated with Liberase TL (Roche) for 15 min at 37 °C. The reaction was stopped by the addition of medium and the mixture was gently dissociated into a single-cell suspension over a 70 µm cell strainer. Cells were incubated with Zombie Aqua Fixable Viability Dye (BioLegend) in PBS at room temperature followed by incubation with 2.4G2 FcR blocking antibodies (clone 2.4G2; BD Biosciences) in FACS buffer (PBS, 0.5% BSA and 0.2% NaN_3) for 20 min on ice. Cells were then stained with surface markers (Table 2) for 30 min at room temperature. For intracellular staining markers, cells were fixed and stained using the Foxp3/Transcription Factor Staining Buffer Set (eBiosciences) according to manufacturer's instructions. Cells were then washed with FACS buffer and stained with intracellular markers (Table 2) for 60 min at room temperature. Subsequently, cells were washed twice and resuspended in 150 µl for analysis.

Table 2 Antibodies used in immune characterization of tumors by flow cytometry

Marker	Clone	Fluorochrome	Supplier
Surface Markers:			
CD44	IM7	APC-Cy7	Biolegend
TCRyd	GL3	BUV496	BD Biosciences
CD11c	N418	BUV563	BD Biosciences
CD103	2E7	BUV615	BD Biosciences
CD19	1D3	BUV661	BD Biosciences
CD62L	MEL-14	BV421	Biolegend
Ly6C	HK1.4	BV570	Biolegend
CD69	H1.2F3	BV605	Biolegend
NK1.1	PK136	BV650	BD Biosciences
CXCR3	CXCR3-173	BV711	BD Biosciences
PD-1	RMP1-30	FITC	Thermofisher
CD3	145-2C11	PECF594	BD Biosciences
F4/80	BM8	PE-Cy5	Biolegend
KLRG-1	2F1	PE-Cy7	Invitrogen
CD45	30-F11	RealBlue705	BD Biosciences
CD4	CK1,5	RealBlue744	BD Biosciences
CD25	2A3	RealBlue780	BD biosciences
CCR2	475,301	RealYellow586	BD Biosciences
CD11b	M1/70	Spark PLUS UV395	Biolegend
CD8	53−6.7	SparkBlue550	Biolegend
Ly6G	1A8	BUV805	BD Biosciences
CD84	1D3/CD84	BUV737	BD Biosciences
Intracellular Markers:			
iNOS	CXNFT	APC	eBioscience
FoxP3	FJK-16s	PE	eBioscience
CD206	Y17-505	R718	BD Biosciences

Flow cytometry acquisition

Samples acquired using a Sony ID7000 spectral cytometer at the Flow cytometry Core Facility (FCF) of LUMC in Leiden, the Netherlands (https://www.lumc.nl/research/facilities/fcf). Single staining controls were prepared on UltraComp eBeads Plus (ThermoFisher Scientific), incubated 20 min at room temperature with the conjugated antibodies,

washed with FACS buffer and then resuspended in 150 µl of FACS buffer. Stained cells and single stained controls were acquired on a Sony ID7000 spectral cytometer. This cytometer is configured with 5 lasers (355 nm, 405 nm, 488 nm, 561 nm, and 637 nm) and the PMT voltages were set up for each laser independently. Samples were unmixed on id7000 software (Sony). Each dye was assigned a spectrum shape before unmixing was calculated. Unstained cells were analysed using the Autofluorescence Finder tool and autofluorescent cells were gated out.

Statistical and data analyses

For all mice experiments, tumor volume was determined using the following formula: $Width^2 \times Length$. For survival analysis, Kaplan Meier curve analysis and log rank test were performed. Slidescanner ImageJ software [55] was used for the quantification of tissue and organ stainings by using Color Deconvolution H DAB and H&E, and for the quantification of organoid count and area by thresholding and analyzing particles. Flow cytometry data was analyzed using FlowJoTM Software Version 10.1 (Becton, Dickinson and Company). For testing statistical significance, Mann Whitney test and one-way ANOVA with multiple testing were performed.

Ethics approval

Tissues were used in accordance with the Code of Conduct for Responsible Use of human tissues, and after written informed consent was obtained. Approval for this study was obtained from the biobank committee as part of the medical ethics committee of the Leiden University Medical center and registered under protocol RP 24.004. All authors had access to the study data and had reviewed and approved the final version of the manuscript.

Role of funders

This project was supported by the Dutch Cancer Society (KWF Kankerbestrijding) and HealthHolland PPS grants (14974 and 15066) to L.J.A.C.H., H.K., M.G.W.L. and OncoLize. The sources of funding did not influence the design of the study, the collection of data, the analysis of data, the interpretation of results, or the writing of the manuscript.

Supplementary Information The online version contains supplementary material available at https://doi.org/10.1007/s13346-026-02187-6.

Acknowledgements This project was supported by the Dutch Cancer Society (KWF Kankerbestrijding) and HealthHolland PPS grants (14974 and 15066) to L.J.A.C.H., H.K., M.G.W.L. and OncoLize. Animal facility at LUMC is acknowledged for the support of the personnel, materials and infrastructure. Micro-Tech Endoscopy Europe is acknowledged for donating the EUS-FNA devices for injection force testing. Support and efforts from Surgery and Pathology departments at LUMC are highly appreciated and acknowledged. Patients and their families are acknowledged for the participation and crucial role in this study.

Author contributions A.V.M. and A.M. designed and performed in vitro and in vivo experiments, analyzed data, and wrote the manuscript. C.R.S. and L.Z. performed experiments of ChemoGell formulation and characterization. A.A. did all ChemoGell injection force testing. E.J.M. and P.K. performed in vivo experiments. S.G.T.J. contributed to ChemoGell reconstitution. E.J.M, A.M. and A.S.M. performed and contributed to tissue stainings. L.J.A.C.H., T.T., H.M.K. and M.G.W.L. designed and supervised the study and wrote the manuscript.

Funding This project was supported by the Dutch Cancer Society (KWF Kankerbestrijding) and HealthHolland PPS grants (14974 and 15066) to L.J.A.C.H., H.K., M.G.W.L. and OncoLize. The collaboration project is co-funded by PPP allowance made available by Health~Holland, Top Sector Life Sciences & Health, to stimulate public-private partnerships.

Data availability The data that support the findings of this study are available on request from the corresponding author.

Declarations

Competing interests H.M.K is a named inventor on granted patent US20230126053 'Thermo-responsive hydrogel for intratumoral administration as a treatment in solid tumor cancers' and is also co-founder and CSO of OncoLize LLC. M.G.W.L. is co-founder and CEO of OncoLize LLC. T.T. is drug development director of OncoLize LLC. L.J.A.C.H receives consultancy fees from InnoSer BioSciences and has supported grants from Tracon Pharmaceuticals (not related to this work). This work was supported by a research grant from OncoLize to L.J.A.C.H.

References

1. Rahib L, Smith BD, Aizenberg R, Rosenzweig AB, Fleshman JM, Matrisian LM. Projecting Cancer Incidence and Deaths to 2030: The Unexpected Burden of Thyroid, Liver, and Pancreas Cancers in the United States. Cancer Res. 2014;74(11):2913–21.
2. Conroy T, Pfeiffer P, Vilgrain V, Lamarca A, Seufferlein T, O'Reilly EM, et al. Pancreatic cancer: ESMO Clinical Practice

Guideline for diagnosis, treatment and follow-up☆. Ann Oncol. 2023;34(11):987–1002.
3. Stoop TF. Pancreatic cancer. Lancet. 2025;405:1182–202.
4. Conroy T, Hammel P, Hebbar M, Abdelghani MB, Wei AC, Raoul J-L, et al. FOLFIRINOX or Gemcitabine as Adjuvant Therapy for Pancreatic Cancer. N Engl J Med. 2018;379(25):2395–406.
5. Klein-Brill A, Amar-Farkash S, Lawrence G, Collisson EA, Aran D. FOLFIRINOX vs Gemcitabine Plus Nab-Paclitaxel for Metastatic Pancreatic Cancer. JAMA Netw Open. 2022;5(6):e2216199.
6. Chen Y-G, Pan H-H, Dai M-S, Lin C, Lu C-S, Su S-L, et al. Impact of Comorbidity and Age on Determinants Therapeutic Strategies in Advanced Pancreatic Head Cancer Patients With Obstructive Jaundices. Med August. 2015;94(31):e1298.
7. van den Bosch MAAJ, Prevoo W, van der Linden EM, Meijerink MR, van Delden OM, Mali WPTM, et al. [The radiologist as the treating physician for cancer: interventional oncology]. Ned Tijdschr Geneeskd. 2009;153:A532.
8. Ramazani F, Nostrum CFv, Storm G, Kiessling F, Lammers T, Hennink WE, et al. Locoregional cancer therapy using polymer-based drug depots. Drug Discovery Today. 2016;21(4):640–7.
9. Solomon SB, Silverman SG. Imaging in Interventional Oncology1. Radiology. 2010;257(3):624–40.
10. Luo W, Zhang T. The new era of pancreatic cancer treatment: Application of nanotechnology breaking through bottlenecks. Cancer Lett. 2024;594:216979.
11. EP G, AR H, BA A. JS M. Intratumoral cancer chemotherapy and immunotherapy: opportunities for nonsystemic preoperative drug delivery - PubMed. J Pharm Pharmacol. 2002;54(2):159–80.
12. Rossi SM, Ryan BK, Kelly HM, Rossi SM, Ryan BK, Kelly HM. Evaluation of the activity of a chemo-ablative, thermoresponsive hydrogel in a murine xenograft model of lung cancer. Br J Cancer. 2020;123(3):369–77.
13. Zhao J, Wang L, Zhang H, Liao B, Li Y, Zhao J, et al. Progress of Research in In Situ Smart Hydrogels for Local Antitumor Therapy: A Review. Pharmaceutics. 2022;14(10):2028.
14. Kim DY, Kwon DY, Kwon JS, Park JH, Park SH, Oh HJ, et al. Synergistic anti-tumor activity through combinational intratumoral injection of an in-situ injectable drug depot. Biomaterials. 2016;85:232–45.
15. Jhan H-J, Liu J-J, Chen Y-C, Liu D-Z, Sheu M-T, Ho H-O. Novel Injectable Thermosensitive Hydrogels for Delivering Hyaluronic Acid–Doxorubicin Nanocomplexes to Locally Treat Tumors. Nanomedicine. 2015;10(8):1263–74.
16. Sheu M-T, Jhan H-J, Su C-Y, Chen L-C, Chang C-E, Liu D-Z et al. Codelivery of doxorubicin-containing thermosensitive hydrogels incorporated with docetaxel-loaded mixed micelles enhances local cancer therapy. Colloids and Surfaces B: Biointerfaces. 2016;143.
17. Li T, Zhang M, Wang J, Wang T, Yao Y, Zhang X, et al. Thermosensitive Hydrogel Co-loaded with Gold Nanoparticles and Doxorubicin for Effective Chemoradiotherapy. AAPS J. 2015;18(1).
18. Rossi SM, Murray TE, Cassidy J, Lee MJ, Kelly HM, Rossi SM, et al. A Custom Radiopaque Thermoresponsive Chemotherapy-Loaded Hydrogel for Intratumoural Injection: An In Vitro and Ex Vivo Assessment of Imaging Characteristics and Material Properties. Cardiovasc Interventional Radiol. 2018;42(2):289–97.
19. Mini E, Nobili S, Caciagli B, Landini I, Mazzei T. Cellular pharmacology of gemcitabine. Ann Oncol. 2006;17:v7–12.
20. Murphy F, Middleton M. Cytostatic and cytotoxic drugs. Side Eff Drugs Annual. 2012;34:731–47.
21. Plate JM, Plate AE, Shott S, Bograd S, Harris JE. Effect of gemcitabine on immune cells in subjects with adenocarcinoma of the pancreas. Cancer Immunol Immunother. 2005;54(9):915–25.
22. Soeda A, Morita-Hoshi Y, Makiyama H, Morizane C, Ueno H, Ikeda M, et al. Regular Dose of Gemcitabine Induces an Increase in CD14+Monocytes and CD11c+ Dendritic Cells in Patients with Advanced Pancreatic Cancer. Jpn J Clin Oncol. 2009;39(12):797–806.
23. Butenko S, Nagalla RR, Guerrero-Juarez CF, Palomba F, David L-M, Nguyen RQ, et al. Hydrogel crosslinking modulates macrophages, fibroblasts, and their communication, during wound healing. Nat Commun. 2024;15(1).
24. Lencioni G, Gregori A, Toledo B, Rebelo R, Immordino B, Amrutkar M, et al. Unravelling the complexities of resistance mechanism in pancreatic cancer: Insights from in vitro and ex-vivo model systems. Sem Cancer Biol. 2024;106:7217–233.
25. Fakhari A, Anand Subramony J. Engineered in-situ depot-forming hydrogels for intratumoral drug delivery. J Controlled Release. 2015;220:465–75.
26. High RA, Randtke EA, Jones KM, Lindeman LR, Ma JC, Zhang S, et al. Extracellular acidosis differentiates pancreatitis and pancreatic cancer in mouse models using acidoCEST MRI. Neoplasia. 2019;21(11):1085–90.
27. Zoe LH, David SR, Rajabalaya R. Chitosan nanoparticle toxicity: A comprehensive literature review of in vivo and in vitro assessments for medical applications. Toxicol Rep. 2023;11:83–106.
28. Gould S, Scott RC. 2-Hydroxypropyl-β-cyclodextrin (HP-β-CD): A toxicology review. Food Chem Toxicol. 2005;43(10):1451–9.
29. Danson S, Ferry D, Alakhov V, Margison J, Kerr D, Jowle D, et al. Phase I dose escalation and pharmacokinetic study of pluronic polymer-bound doxorubicin (SP1049C) in patients with advanced cancer. Br J Cancer. 2004;90(11):2085–91.
30. SD S-J VCM. Safety assessment of poloxamers 101, 105, 108, 122, 123, 124, 181, 182, 183, 184, 185, 188, 212, 215, 217, 231, 234, 235, 237, 238, 282, 284, 288, 331, 333, 334, 335, 338, 401, 402, 403, and 407, poloxamer 105 benzoate, and poloxamer 182 dibenzoate as used in cosmetics. Int J Toxicol. 2008;27:93–128.
31. Deer T, Hedman T, Singh H, Yu J. ID: 325486 Lumbar Intervertebral Joint Stabilization by Injectable Load-Sharing Polymers - Early Clinical Results. Neuromodulation: Technol Neural Interface. 2024;27(7):S38.
32. Cui Z, Li Z, Dong W, Qiu L, Zhang J, Wang S. Comprehensive Metabolite Identification of Genipin in Rats Using Ultra-High-Performance Liquid Chromatography Coupled with High Resolution Mass Spectrometry. Molecules. 2023;28(17):6307.
33. Larson AC, Doty KR, Solheim JC. The double life of a chemotherapy drug: Immunomodulatory functions of gemcitabine in cancer. Cancer Med. 2024;13(10):e7287.
34. Yang Y-L, Yang F, Huang Z-Q, Li Y-Y, Shi H-Y, Sun Q, et al. T cells, NK cells, and tumor-associated macrophages in cancer immunotherapy and the current state of the art of drug delivery systems. Front Immunol. 2023;14:1199173.
35. Palmer N, Khakoo S, Sanchez-Elsner T, Vallejo AF. Enhancing natural killer cell anti-tumour activity through macrophage manipulation. Front Immunol. 2025;16:1656925.
36. Zhang W, Li S, Liu Y, Xing R, Jin Z, Yan X, et al. Immunosuppressive microenvironment improvement and treatment of aggressive malignancy pancreatic ductal adenocarcinoma based on local administration of injectable hydrogel. Nano Today. 2023;50:114423.
37. Zhou H, Wang W, Cai Z, Jia Z-Y, Li Y-Y, He W, et al. Injectable hybrid hydrogels enable enhanced combination chemotherapy and roused anti-tumor immunity in the synergistic treatment of pancreatic ductal adenocarcinoma. J Nanobiotechnol. 2024;22(1):353.
38. Muñoz NM, Williams M, Dixon K, Dupuis C, McWatters A, Avritscher R, et al. Influence of injection technique, drug formulation and tumor microenvironment on intratumoral immunotherapy delivery and efficacy. J Immunother Cancer. 2021;9(2):e001800.

39. Raskov H, Orhan A, Christensen JP, Gögenur I, Raskov H, Orhan A, et al. Cytotoxic CD8+T cells in cancer and cancer immunotherapy. Br J Cancer. 2020;124(2):359–67.
40. Cho YS. Genipin, an Inhibitor of UCP2 as a Promising New Anticancer Agent: A Review of the Literature. Int J Mol Sci. 2022;23(10):5637.
41. Chung CK, García-Couce J, Campos Y, Kralisch D, Bierau K, Chan A, et al. Doxorubicin Loaded Poloxamer Thermosensitive Hydrogels: Chemical, Pharmacological and Biological Evaluation. Molecules. 2020;25(9):2219.
42. Hewitt MJ, McPhail MJ, Possamai L, Dhar A, Vlavianos P, Monahan KJ. EUS-guided FNA for diagnosis of solid pancreatic neoplasms: a meta-analysis. Gastrointest Endosc. 2012;75(2):319–31.
43. Kaur J, Jaruvongvanich V, Chandrasekhara V. Endoscopic ultrasound-guided injectable therapy for pancreatic cancer: A systematic review. World J Gastroenterol. 2022;28(21):2383.
44. Lazarovits J, Epelbaum R, Lachter J, Amikam Y, Arie JB, Lazarovits J, et al. Multisite Is Superior to Single-Site Intratumoral Chemotherapy to Retard the Outcomes of Pancreatic Ductal Adenocarcinoma in a Murine Model. Cancers. 2023;15(24):5801.
45. V E, vD JL, S M, J QP, G K, A-V JM, et al. Neoadjuvant Chemoradiotherapy Versus Upfront Surgery for Resectable and Borderline Resectable Pancreatic Cancer: Long-Term Results of the Dutch Randomized PREOPANC Trial. J Clin Oncol. 2022;40(11).
46. Sharma NR, Lo SK, Hendifar A, Othman MO, Patel K, Mendoza-Ladd A, et al. Response of Locally Advanced Pancreatic Cancer to Intratumoral Injection of Large Surface Area Microparticle Paclitaxel: Initial Report of Safety and Clinical Outcome. Pancreas. 2023;52(3):e179–87.
47. Hirooka Y, Kasuya H, Ishikawa T, Kawashima H, Ohno E, Villalobos IB, Naoe Y, Ichinose T, Koyama N, Tanaka M, Kodera Y. A Phase I clinical trial of EUS-guided intratumoral injection of the oncolytic virus, HF10 for unresectable locally advanced pancreatic cancer. BMC Cancer. 2018;18(1):596.
48. Stoop TF, Theijse RT, Seelen LWF, Groot Koerkamp B, van Eijck CHJ, Wolfgang CL, et al. Preoperative chemotherapy, radiotherapy and surgical decision-making in patients with borderline resectable and locally advanced pancreatic cancer. Nat Reviews Gastroenterol Hepatol. 2023;21(2).
49. Beutel AK, Halbrook CJ. Barriers and opportunities for gemcitabine in pancreatic cancer therapy. Am J Physiology-Cell Physiol. 2023;324(2):C540–52.
50. Groeneveldt C, Kinderman P, Wollenberg DJMvd O, RLvd, Middelburg J, Mustafa DAM, et al. Preconditioning of the tumor microenvironment with oncolytic reovirus converts CD3-bispecific antibody treatment into effective immunotherapy. J Immunother Cancer. 2020;8(2):e001191.
51. Schoonderwoerd MJA, Hakuno SK, Sassen M, Kuhlemaijer EB, Paauwe M, Slingerland M, et al. Targeting Endoglin Expressing Cells in the Tumor Microenvironment Does Not Inhibit Tumor Growth in a Pancreatic Cancer Mouse Model. OncoTargets Therapy. 2021;14:5205–20.
52. Boj SF, Hwang CI, Baker LA, Chio II, Engle DD, Corbo V, Jager M, Ponz-Sarvise M, Tiriac H, Spector MS, Gracanin A. Organoid models of human and mouse ductal pancreatic cancer. Cell. 2015;160(1):324–38.
53. Harryvan TJ, Hawinkels LJAC, Östman A, Dijke Pt, Strell C, Hornsveld M. A Novel Pancreatic Cancer Mini-tumor Model to Study Desmoplasia and Myofibroblastic Cancer-Associated Fibroblast Differentiation. Gastro Hep Adv. 2022;1(4):678–81.
54. Rossomacha E, Hoemanni CD, Shive MS. Simple Methods for Staining Chitosan in Biotechnological Applications. J Histotechnology. 2004;27(1):31–6.
55. Schindelin J, Arganda-Carreras I, Frise E, Kaynig V, Longair M, Pietzsch T, et al. Fiji: an open-source platform for biological-image analysis. Nat Methods. 2012;9(7).